Title: c-Jun N-terminal kinase (JNK) signaling contributes to cystic burden in polycystic kidney disease

Short Title: JNK drives cystic kidney disease

Abigail O. Smith[1 ID], Julie A. Jonassen[2 ID], Kenley M. Preval[1 ID], Roger J. Davis[1 ID], and Gregory J. Pazour[1*ID]

[1]Program in Molecular Medicine, University of Massachusetts Medical School, Biotech II, Suite 213, 373 Plantation Street, Worcester, MA, USA 01605

[2]Department of Microbiology and Physiological Systems, University of Massachusetts Medical School, 55 Lake Avenue North, Worcester MA 01655

*Correspondence to: Telephone: 508 856 8078, Email: gregory.pazour@umassmed.edu

ID
AOS: https://orcid.org/0000-0003-2765-8737
JAJ: https://orcid.org/0000-0001-9997-2069
KMP: https://orcid.org/0000-0002-2425-0878
RJD: https://orcid.org/0000-0002-0130-1652
GJP: https://orcid.org/0000-0002-6285-8796

Key words:

Abbreviations: PKD, polycystic kidney disease; ADPKD, autosomal dominant polycystic kidney disease; JNK, jun N-terminal kinase; cAMP, cyclic adenosine monophosphate; AP-1, activator protein-1; H&E, Hematoxylin and eosin; LTA, Lotus tetragonolobus agglutinin; DBA, Dolichos biflorus agglutinin; MAP, mitogen-activated protein; MAP2K, mitogen-activated protein kinase kinase; MAP3K, mitogen-activated protein kinase kinase kinase; SMA, alpha smooth muscle actin; DAPI, 4',6-diamidino-2-phenylindole; GPCR, G-protein coupled receptor

Abstract

Polycystic kidney disease is an inherited degenerative disease in which the uriniferous tubules are replaced by expanding fluid-filled cysts that ultimately destroy organ function. Autosomal dominant polycystic kidney disease (ADPKD) is the most common form, afflicting approximately 1 in 1,000 people. It primarily is caused by mutations in the transmembrane proteins polycystin-1 (Pkd1) and polycystin-2 (Pkd2). The most proximal effects of *Pkd* mutations leading to cyst formation are not known, but pro-proliferative signaling must be involved for the tubule epithelial cells to increase in number over time. The c-Jun N-terminal kinase (JNK) pathway promotes proliferation and is activated in acute and chronic kidney diseases. Using a mouse model of cystic kidney disease caused by *Pkd2* loss, we observe JNK activation in cystic kidneys and observe increased nuclear phospho c-Jun in cystic epithelium. Genetic removal of *Jnk1* and *Jnk2* suppresses the nuclear accumulation of phospho c-Jun, reduces proliferation and reduces the severity of cystic disease. While *Jnk1* and *Jnk2* are thought to have largely overlapping functions, we find that *Jnk1* loss is nearly as effective as the double loss of *Jnk1* and *Jnk2*. Jnk pathway inhibitors are in development for neurodegeneration, cancer, and fibrotic diseases. Our work suggests that the JNK pathway should be explored as a therapeutic target for ADPKD.

Author Summary

Autosomal dominant polycystic kidney disease is a leading cause of end stage renal disease requiring dialysis or kidney transplant. During disease development, the cells lining the kidney tubules proliferate. This proliferation transforms normally small diameter tubules into fluid-filled cysts that enlarge with time, eventually destroying all kidney function. Despite decades of research, polycystic kidney disease remains incurable. Furthermore, the precise signaling events involved in cyst initiation and growth remain unclear. The c-Jun N-terminal kinase (JNK), is a major pathway regulating cellular proliferation and differentiation but its importance to polycystic kidney disease was not known. We show that JNK activity is elevated in cystic kidneys and that reducing JNK activity decreases cyst growth pointing to JNK inhibition as a therapeutic strategy for treating polycystic kidney disease.

Introduction

Autosomal dominant polycystic kidney disease (ADPKD) is the most common form of inherited kidney disease, afflicting approximately 1 in 1,000 people in the United States and worldwide. Patients with ADPKD exhibit gradual kidney function decline due to uncontrolled epithelial cell proliferation and secretion that transforms narrow uriniferous tubules into large, fluid-filled cysts. The majority of ADPKD cases are due to mutations in either of two transmembrane proteins, polycystin-1 (Pkd1) and polycystin-2 (Pkd2), that form a heterotetrameric complex in the primary ciliary membranes [1]. It is widely believed that perturbing this ciliary complex, either by loss-of-function mutations or disrupting cilia structure triggers the cellular phenotype that leads to cyst formation [2-4]. Although the precise mechanism by which the polycystin complex preserves tubule architecture remains obscure, some aspects of pro-cystic signaling have been established. For example, Pkd1 or Pkd2 loss leads to reduced intracellular calcium and, subsequently, an abnormal cellular response to cyclic adenosine monophosphate (cAMP) levels [5-7]. In mutant epithelial cells, elevated cAMP promotes increased fluid secretion and epithelial cell proliferation [8]. cAMP reduction via vasopressin 2 receptor antagonism is the mechanism of action of tolvaptan, the single FDA-approved drug for patients with ADPKD [9, 10]. Unfortunately, tolvaptan slows but does not halt disease progression and is not appropriate for all ADPKD patients due to side effects [11]. To improve treatments for ADPKD, we must search for alternative pro-cystic signaling pathways.

Prior studies showed that the c-Jun N-terminal kinase (JNK) signaling pathway is activated in cells overexpressing exogenous Pkd1 [12, 13] or Pkd2 [14] constructs. A later study found the opposite, that Pkd1 loss activated JNK signaling, while Pkd1 overexpression repressed JNK activity [15]. Reports of JNK activity in cystic tissues are also conflicting [16, 17], and no follow-up studies established JNK's role in cyst formation. JNK is a member of the MAP kinase family, which also includes Erk1/2, p38, and Erk5. JNK pathway activators include extracellular stimuli such as UV irradiation, osmotic stress, and cytokines that initiate an intracellular phosphorylation cascade through upstream MAP kinase kinase kinases (MAP3K). Jnk-associated MAP3Ks converge on two MAP kinase kinases (MAP2Ks), Mkk4 and Mkk7. The MAP2Ks phosphorylate MAP kinases including the Jnk paralogs: Jnk1 (Mapk8), Jnk2 (Mapk9), and Jnk3

(Mapk10). Jnk1 and Jnk2 are ubiquitously expressed, while Jnk3 expression is restricted primarily to the central nervous system and testis [18]. Although Jnks have a wide array of substrates, the most studied are the activator protein-1 (AP-1) transcription factors, particularly c-Jun, for which the pathway is named. Increased AP-1 levels have been detected in cystic kidneys in humans and mice [16]. Furthermore, AP-1 promotes proliferation and cell survival by regulating oncogene transcription [19] including *c-Myc*, which was recently shown to contribute directly to cystic kidney disease [20, 21].

JNK activation has been detected in many forms of kidney disease [22]. In animal models, JNK inhibition prior to ischemia-reperfusion or tubule obstruction reduces inflammation and fibrosis, and preserves kidney function [23-27]. Interestingly, acute kidney injury exacerbates polycystic kidney disease [28-30]. In chronic kidney insult, progressive interstitial fibrosis contributes to organ failure. JNK inhibition reduces pro-fibrotic factors in the kidney [26, 27]. Furthermore, researchers produced severe kidney fibrosis in mice by overexpressing the JNK target *c-Jun* [31].

This study aimed to investigate the role of JNK signaling in ADPKD using *in vivo* models to genetically perturb the pathway. Here we show that *Pkd2* deletion increases JNK activation, which contributes to cystic kidneys in young animals and cystic liver in older animals. Jnk1 is more important to the phenotype development than is Jnk2. Overall, our results encourage further investigation of the JNK pathway as a novel therapeutic candidate for treating ADPKD.

Methods

Mouse Studies

The following mouse strains have been described previously: $Pkd2^{fl}$ [32], $Jnk1^{fl}$ [33], $Jnk2^{null}$ [34], $Rosa26\text{-}Cre^{ERT2}$ [35], $Ask1^{-/-}$ [36], $Mlk2^{-/-}$ [37] and $Mlk3^{-/-}$ [38]. The *Ask1* (B6.129S4-Map3k5<tm1Hijo>) mouse was provided by the RIKEN BRC through the National Bio-Resource Project of MEXT, Japan. *Stra8-iCre* [39] was used to convert $Jnk1^{fl}$ to $Jnk1^{null}$. All mice were maintained on a C57BL/6J genetic background. These studies were approved by the Institutional Animal Care and Use Committee of the University of Massachusetts Medical School.

For juvenile onset disease model, mothers were dosed with tamoxifen (200 mg/kg) by oral gavage on postnatal days 2, 3, and 4. The pups remained with nursing mothers until euthanasia at postnatal day 21. For the adult-onset disease model, animals were treated with tamoxifen (50 mg/kg) by intraperitoneal injection on postnatal days 21, 22, and 23. Mice were euthanized 24 weeks after first injection. Both sexes were used in all studies.

Histology

Tissues were fixed by immersion overnight in 10% formalin (Electron Microscopy Sciences) in phosphate-buffered saline and then embedded in paraffin. Sections were deparaffinized and stained with hematoxylin and eosin (H&E) or one-step trichrome. Images of stained sections were obtained with a Zeiss Axio Scan.Z1 slide scanner with brightfield capabilities using the 20X objective. Cystic index was calculated using ImageJ software to outline kidney sections, apply a mask to differentiate cystic from non-cystic regions, and measure the two-dimensional areas. Cystic index = cystic area/total kidney area x 100%.

For immunofluorescent staining, sections were deparaffinized, antigens were retrieved by autoclaving for 30 min in 10 mM sodium citrate, pH 6.0 and stained with primary antibodies diluted in TBST (10 mM Tris, pH 7.5, 167 mM NaCl, and 0.05% Tween 20) plus 0.1% cold water fish skin gelatin (Sigma-Aldrich). Alexa Fluor–labeled secondary antibodies (Invitrogen) were used to detect the primary antibodies. Primary antibodies used included aquaporin 2 (1:100; Sigma # 5200110), phospho S63 c-Jun (1:1000, Cell Signaling Technology), phospho S10 histone H3 (1:250; Millipore # 06570), SMA (1:50,000, Sigma # A5228). FITC-conjugated lectins were added with secondary antibodies: Lotus tetragonolobus agglutinin (LTA, 1:50, Vector Labs) and Dolichos biflorus agglutinin (DBA, 1:20, Vector Labs). Nuclei were labeled with 4’,6-diamidino-2-phenylindole (DAPI). Fluorescent images were obtained with a Zeiss LSM900+ Airyscan microscope. Fluorescent slide scans for Figure 1A and Figure 5A were obtained using Zeiss Axio Scan.Z1 slide scanner.

Gene expression

Kidneys were stored at -80C in RNAlater (Qiagen) until RNA was isolated. For total RNA isolation, tissues were homogenized using TissueLyser II (Qiagen) and RNA isolated using the

RNeasy Mini Kit (Qiagen). cDNA was synthesized using SuperScript II Reverse Transcription (Invitrogen). Real time quantitative PCR was performed with KAPA SYBR FAST Universal reagent (Roche) using an Eppendorf Realplex2 cycler. All qPCR reactions were performed in triplicate and melting curves verified that a single product was amplified. Standard curves were generated by 5-fold serial dilutions of a pool of untreated mouse kidney cDNA, and for each gene, the threshold cycle was related to log cDNA dilution by linear regression analysis. Gene expression data were normalized to glyceraldehyde-3-phosphate dehydrogenase expression. The following primers were used: *Pkd2 forward* CGAGGAGGAGGATGACGAAGAC; *Pkd2 reverse* TGGAAACGATGCTGCCAATGGA; *Gapdh forward* GCAATGCATCCTGCACCACCA; *Gapdh reverse* TTCCAGAGGGGCCATCCACA.

Immunoblotting

For Figure 1 only, kidneys stored in RNAlater were homogenized in Buffer RLT (RNeasy MiniKit, Qiagen). Protein was precipitated from the supernatant by adding 9 volumes of 100% methanol, collected by centrifugation at 3,000xg for 10 min at 4C followed by three washes in 90% methanol. Protein pellets were reconstituted in 2X SDS-PAGE loading buffer. In all other experiments, frozen kidneys were homogenized in ice-cold RIPA buffer (150 mM NaCl, 1% Triton X-100, 0.05% sodium deoxycholate, 0.01% SDS, 50 mM Tris-HCl, pH 7.5) supplemented with Complete Mini EDTA-free Protease Inhibitor cocktail tablets (Roche), sodium orthovanadate (0.5 mM), sodium fluoride (10 mM), and phenylmethylsulfonyl fluoride (1 mM). Equal amounts of protein were loaded and separated in 12% SDS-PAGE gels and transferred to Immobilon-FL PVDF membranes (Millipore). Membranes were blocked for 1 hour at room temperature with Intercept (TBS) Blocking Buffer (Li-Cor) or 5% non-fat dry milk in TBST followed by incubation with primary antibodies overnight at 4C.

The following antibodies were used: JNK1/2 (1:1000, BD Pharmingen # 554285), c-Jun (1:200, Santa Cruz Biotechnology # 74543), phospho T183/Y185 SAPK/JNK (1:1000, Cell Signaling Technology # 9251), phospho S63 c-Jun (1:1000, Cell Signaling Technology # 9261), glyceraldehyde-3-phosphate dehydrogenase (1:10,000, Proteintech, 60004-1-Ig), SMA (1:1,000, Sigma # A5228), glyceraldehyde-3-phosphate dehydrogenase (1:1,000, Cell Signaling Technology # 3683S), phospho T180/Y182 p38, (Cell Signaling Technology # 9211). Primary

antibodies were detected using near infrared secondary antibodies (Li-Cor) and blots were imaged on Odyssey Li-Cor imager. Quantification was performed using Image Studio Lite software.

Results

Postnatal deletion of *Pkd2* activates JNK signaling in juvenile mouse kidneys.

To assess JNK signaling in an *in vivo* ADPKD model, we induced *Pkd2* deletion in postnatal mice by the tamoxifen inducible RosaCre^{ERT2} driver. This widely expressed Cre causes gene deletion in most cells, including kidney tubule epithelium [40, 41]. We administered tamoxifen via maternal oral gavage on postnatal (P) days 2-4 and harvested on P21. Treating *Pkd2 flox* (*fl*) homozygotes (*Rosa26-Cre^{ERT2}; Pkd2$^{fl/fl}$*) resulted in extensive kidney cysts. In contrast, heterozygous mice (*Rosa26-Cre^{ERT2}; Pkd2$^{fl/+}$)* similarly treated, exhibited no cysts and thus served as controls (Figure 1A).

Total Jnk protein in *Pkd2* mutant kidneys was unchanged compared to controls but phosphorylated Jnk was significantly increased (Figure 1B-D). These antibodies recognize both Jnk1 and Jnk2, each of which is alternatively spliced to generate 54 kDa and 46 kDa products (Supplemental Figure 3A). Pkd2 loss did not significantly alter total c-Jun levels, but did elevate phosphorylated c-Jun (Figure 1B, E-F). Our findings indicate that *Pkd2* deletion activates JNK signaling and could drive cyst formation.

JNK inhibition reduces severity of cystic phenotype in juvenile *Pkd2* mutant mice.

Our finding that the loss of Pkd2 activates JNK signaling could indicate that JNK activation drives cyst formation, or cyst formation could activate JNK signaling. To distinguish these possibilities, we tested how JNK inhibition affects cyst formation driven by Pkd2 loss. Mice express three Jnk paralogs. *Jnk1* and *Jnk2* are widely expressed including in kidney, while *Jnk3* is limited to brain and testis [18]. Thus, we focused on *Jnk1* and *Jnk2*. Losing both genes causes embryonic lethality. To circumvent lethality, we intercrossed parents carrying germline *Jnk2* deletions and floxed *Jnk1* alleles with *Pkd2^{fl}; Rosa26-Cre^{ERT2}* alleles used previously. Offspring, carrying assorted alleles, were treated with tamoxifen on P2-4, harvested on P21, and genotyped (Figure 2). *Pkd2* heterozygotes carrying any number of wild-type *Jnk* alleles had normal kidney to body

198 weight and no evidence of structural abnormalities or cysts. Kidneys lacking *Pkd2* but carrying
199 at least one wild-type allele of *Jnk1* and *Jnk2* showed severe cystic disease similar to *Pkd2*
200 deletion alone. Kidneys lacking *Pkd2* and all functional *Jnk* alleles had a 23% reduction in two-
201 kidney to body weight and a 16% reduction in cystic index (Figure 2B-C). Hematoxylin and eosin
202 (H&E) stained mid-sagittal sections revealed large cysts at the cortical-medullary boundary and
203 smaller cysts in the cortex and medulla in *Pkd2* mutants with intact JNK activity. *Jnk* deletion
204 reduced cysts in the cortex and medulla. Cysts remained at the cortical-medullary boundary but
205 were less extensive (Figure 2A). Our observation that *Jnk* deletion reduces disease severity
206 supports the hypothesis that JNK activation contributes to cystic disease.

207 We observed variability in kidney to body weight in *Pkd2* mutants (Figure 2B). We
208 hypothesized that this was due to variation in *Pkd2* levels after Cre-mediated deletion. To test
209 our hypothesis, we measured *Pkd2* mRNA levels by RT-qPCR and normalized to *Gapdh*. Non-
210 cystic controls (*Rosa26-Cre*^{ERT2}; *Pkd2*$^{fl/+}$) used throughout this study, are expected to have about
211 one half as much *Pkd2* message as Cre-negative animals and this was observed (Supplemental
212 Figure 1). Cystic groups (*Rosa26-Cre*^{ERT2}; *Pkd2*$^{fl/fl}$) with or without JNK activity showed reduced
213 *Pkd2* mRNA levels compared to non-cystic controls but the reduction did not reach significance
214 due to variation between animals. Importantly, we found similar variation and no difference in
215 mean *Pkd2* mRNA levels in *Pkd2* mutants with and without Jnk alleles. This finding indicates
216 that the difference in cystic burden between *Pkd2* mutants with and without JNK activity is not
217 due to systematic differences in *Pkd2* levels.

218 Multiple upstream MAP3Ks activate JNK. Identifying and inhibiting relevant MAP3Ks in
219 the context of cystic kidney disease could be therapeutically beneficial. To this end, we selected
220 three MAP3K genes, *Ask1 (Map3k5)*, *Mlk2 (Map3k10),* and *Mlk3 (Map3k11)*, with connections
221 to kidney disease for further analysis. *Ask1* inhibition reduces kidney and liver fibrosis [42].
222 Cdc42 and Rac1 mediate JNK activation in the context of polycystin overexpression in cells [12,
223 14] and activate *Mlk2* and *Mlk3* [37, 43, 44]. However, in our model, *Ask1* deletion
224 (Supplemental Figure 2A) or double deletion of *Mlk2* and *Mlk3* (Supplemental Figure 2B) did
225 not reduce cystic burden in *Pkd2* mutants. Thus, identifying relevant MAP3Ks will require
226 further investigation.

Pkd2 deletion activates the transcription factor c-Jun in kidney tubule epithelial cells.

The c-Jun subunit of the AP-1 transcription factor complex is dually phosphorylated by Jnk on serines 63 and 73 [45]. To detect nuclear-localized phosphorylated c-Jun, indicating JNK activation, we probed kidney sections for phospho S63 c-Jun. In control kidneys, we found no positive nuclei in proximal tubule cells (defined by LTA staining) or collecting duct cells (defined by DBA staining) (Figure 3). Cystic kidneys due to *Pkd2* loss exhibited extensive phospho S63 c-Jun nuclear staining in both proximal tubules and collecting ducts. Consistent with most cysts in this model deriving from collecting ducts, we observed more phospho S63 c-Jun positive cells in DBA-positive tubules compared to LTA-positive tubules. *Jnk* deletion reduced phospho S63 c-Jun positive cells nearly to wild type levels (Figure 3). Our findings confirm that JNK activation occurs in the tubule epithelium and correlates positively with regions of increased cyst formation.

JNK inhibition reduces tubule epithelial cell proliferation in juvenile _Pkd2_ mutant mice.

Cyst growth depends on tubule epithelial cell proliferation, and a recent study found differential expression of cell cycle genes in *Pkd2* mutant mouse kidneys [46]. To determine whether *Jnk* deletion reduces tubule cell proliferation in *Pkd2* mutant kidneys, we probed tissue sections for the mitotic marker phospho S10 histone H3 (Figure 4). As expected, *Pkd2* mutant kidneys showed markedly increased proliferation compared to wild type. Proximal tubule cell proliferation nearly doubled from 2.3% in wild-type kidneys to 4.3% in *Pkd2* kidneys. *Jnk* deletion returned the rate to wild-type levels (Figure 4B). In collecting ducts, proliferation was nearly ten times higher in *Pkd2* mutants compared to wild type and *Jnk* deletion reduced proliferation by 43% (Figure 4C). These findings suggest that JNK inhibition reduces cyst formation by inhibiting tubule epithelial cell proliferation.

JNK inhibition reduces fibrosis in juvenile _Pkd2_ mutant mice.

JNK signaling promotes interstitial fibrosis in non-cystic kidney disease models [25, 26]. As fibrosis also contributes to advanced cystic kidney disease [47], we hypothesized that *Jnk* deletion may reduce fibrosis in *Pkd2* mutants. To measure fibrosis, we stained kidney sections for alpha-smooth muscle actin (SMA), a marker of active myofibroblasts (Figure 5). As expected, SMA staining was restricted to perivascular regions in wild-type kidneys. In contrast, *Pkd2*

mutants exhibited significant SMA expression surrounding cystic and non-cystic tubules while *Pkd2* mutants lacking JNK activity had decreased SMA staining (Figure 5A-B) and reduced SMA protein levels (Figure 5C-D). Thus, JNK inhibition reduces interstitial fibrosis in *Pkd2* mutant kidneys.

Jnk1 is primarily responsible for reducing cystic disease in juvenile _Pkd2_ mutant kidneys.

Jnk1 and *Jnk2* are largely redundant in development but their roles diverge in adult tissues in a complex manner that is incompletely understood, yet critical for developing JNK inhibitor therapies [48, 49]. To determine how each *Jnk* gene contributes to cysts, we crossed parents carrying $Pkd2^{fl}$; $Rosa26\text{-}Cre^{ERT2}$ alleles and germline $Jnk2^{null}$ or $Jnk1^{null}$ alleles. We treated mice as in Figure 2. Trichrome staining revealed that *Pkd2* heterozygotes were non-cystic with normal collagen deposition (Figure 6A). In contrast, *Pkd2* mutants contained large cysts at the cortical-medullary boundary and smaller cysts throughout. Collagen deposits were notable at the outer medulla and cyst boundaries. As shown in Figure 2, complete JNK deletion reduced cortical-medullary cysts. Collagen staining was visible but reduced. *Pkd2* mutants lacking only *Jnk1* exhibited fewer cysts and less fibrosis than *Pkd2* mutants with intact JNK. In contrast, *Pkd2* mutants lacking only *Jnk2* resembled cystic *Pkd2* mutants with JNK signaling intact. Kidney to body weight ratios and cystic indices support the histological evidence that *Jnk1* deletion reduces cysts more than *Jnk2* deletion (Figure 6B-C).

Immunoblots revealed increased c-Jun phosphorylation in *Pkd2* mutants (Figure 6D-E). Combined *Jnk1* and *Jnk2* deletion reduced phospho S63 c-Jun to near wild-type levels. *Jnk1* deletion also reduced phospho S63 c-Jun to near wild-type levels while *Jnk2* deletion did not. Our findings complement a recent study in which *Jnk1* deletion, but not *Jnk2* deletion, limited ischemia-reperfusion injury in mouse kidneys [23].

To measure Jnk isoform expression and phosphorylation, we probed immunoblots with antibodies against total and phosphorylated Jnk (Supplemental Figure 3A). Two independent splicing events generate four isoforms each from Jnk1 and Jnk2. One site regulates inclusion of mutually exclusive exon 6a/6b, however these forms are not distinguishable by immunoblot. The other dictates choice of a C-terminal coding exon yielding long (p54) and short (p46)

isoforms of both *Jnk1* and *Jnk2,* which can be distinguished by immunoblot (Supplemental Figure 3A). Dual phosphorylation at Thr-Pro-Tyr activates all Jnk isoforms [50, 51], and we detected increased phosphorylation of p54 and p46 in *Pkd2* mutant kidneys (Supplemental Figure 3A, 3C). *Jnk2* deletion alone reduced p54 and phospho-p54 as effectively as total *Jnk* deletion. However, *Jnk1* deletion had no effect, suggesting p54 derives mostly from Jnk2. *Jnk1* and *Jnk2* single deletions reduced phospho-p46, suggesting p46 derives from both genes. We detected a third band (p45), whose phosphorylation was elevated in all *Pkd2* mutants including those lacking Jnk1 or Jnk2. The observation that p45 remains in both *Jnk1* and *Jnk2* mutants suggests that it can be generated from either gene perhaps through a yet undescribed splicing event or a post translational modification. Alternatively, p45 could arise from antibody cross-reactivity with a different protein. Possibly, MAP kinase p38, as p38's phosphorylation pattern matches p45 (Supplemental Figure 3D) however, p38 migrates faster than p45 making this unlikely. Our results show that *Pkd2* loss induces phosphorylation of long and short isoforms of Jnk1 and Jnk2, but *Jnk1* is the critical enzyme for cystic disease.

JNK deletion reduces severity of cystic liver disease in adult *Pkd2* mutant mice.

Inhibiting JNK signaling reduced cystic kidney disease in a rapidly progressing model of ADPKD. However, humans with ADPKD accumulate cysts over decades. Thus, we wanted to evaluate JNK signaling in a slowly progressing disease model. In mice, timing of cystic gene deletion determines rate of disease progression. *Pkd1* loss prior to P13 causes cyst accumulation within weeks, while deletion after P14 delays cysts for 5-6 months [52, 53]. For our slow-progressing model, we delivered tamoxifen at P21-23. *Pkd2* mutants aged 6 months showed no signs of kidney cysts in histological sections or by 2-kidney to body weight ratios (Supplemental Figure 4). Segregation by sex revealed no differences between *Pkd2* mutants with or without *Jnk* (Supplemental Figure 5). We expect that *Pkd2* mutants would develop kidney cysts at older ages based on evidence from *Pkd1* models [52], but severe liver findings (Figure 7) precluded further aging.

Polycystic liver disease is the most common extrarenal ADPKD symptom [54]. Interestingly, despite lacking kidney cysts, adult *Pkd2* mutants contained numerous biliary liver cysts. Livers were enlarged and indurated, with visible fluid-filled cysts causing a yellowish hue

(Figure 7B). Trichrome staining showed extensive cystic and fibrotic changes throughout, with rare areas of healthy tissue. We observed numerous small and occasional large cysts, frequently surrounded by collagen (Figure 7A). JNK inhibition significantly improved liver cysts, reducing liver to body weight ratio by 38% (Figure 7C). Polycystic liver disease is more prevalent in females than males [55], but all mice in our study developed liver cysts after *Pkd2* deletion with no difference between males and females (Supplemental Figure 5). JNK-deleted cystic livers were smaller and remained indurated and pale (Figure 7B) with reduced cysts and fibrosis (Figure 7A). In addition to driving cyst progression in juvenile *Pkd2* mutant kidneys, JNK signaling also contributes to cyst progression in adult *Pkd2* mutant livers.

Discussion

Improving ADPKD treatment requires understanding signaling downstream of the polycystins. We investigated JNK's role in promoting cysts due to Pkd2 loss and found that disrupting JNK signaling reduced kidney cysts in juvenile mice and liver cysts in adult mice. Our findings invite further exploration of JNK as a therapeutic target for ADPKD. JNK inhibitors have successfully treated liver and kidney disease in animals [24-26, 56-58]. Unfortunately, toxic effects ended multiple human clinical trials [59] suggesting that JNK inhibition would not be appropriate in chronic conditions like ADPKD. However, it is expected that the loss of Pkd2 would activate a MAP3K upstream of JNK. MAP3K inhibitors are in development as clinical reagents, and these do not show the toxic effects of Jnk inhibitors [60-64] making them more appropriate for ADPKD. Of course, identification of the relevant MAP3K is required. Mouse and human genomes encode 24 MAP3Ks, with at least 14 known to phosphorylate Mkk4 or Mkk7 upstream of Jnks [18, 65]. Our studies suggest that Ask1, Mlk2 and Mlk3 are not relevant, leaving the critical MAP3K still to be identified.

MAPK signaling is typically activated by receptor tyrosine kinases, GPCRs and other membrane receptors detecting stress, cytokines, growth factors and other agonists. Signals are often propagated to the MAP3Ks by the action of Rac1 and Cdc42. Overexpression of Pkd2 or the C-terminal tail of Pkd1 can activate JNK and dominant negative mutations of Rac1 and Cdc42 block the activation [12, 14]. These observations suggest that the polycystins act

upstream of MAP3Ks, but the mechanism is unknown. Polycystins can function as atypical GPCRs to activate heterotrimeric G proteins [13, 15, 66] suggesting a possible mechanism. Alternatively, less direct mechanisms such as altered calcium signaling could be involved. Polycystin mutations are known to reduce cellular calcium and calcium levels can regulate JNK through PI3K/Akt [67].

The protective effect of JNK inhibition on cystic disease is driven by *Jnk1*. Jnk1 and Jnk2 are structurally similar [50] and have overlapping functions. However, evidence suggests distinct and even opposing roles for Jnks in tissue homeostasis and cancer [68, 69]. Functional differences between Jnk1 and Jnk2 may be due to alternative processing of their transcripts. Two independent splicing events produce four distinct isoforms of both genes. One event alters the open reading frame at the C-terminus [50] and has unknown consequences to protein function. Another event dictates inclusion of mutually exclusive exons 6a/6b (mice) or 7a/7b (humans) within the kinase domain and appears to affect kinase activity [70]. Jnk splicing in mouse kidney is uncharacterized, but the Jnk1 and Jnk2 produced in kidney may contain different versions of exon 6, which could influence isoform activity or substrate specificity.

94% of ADPKD patients develop hepatic cysts by their fourth decade, but most remain asymptomatic [71]. Rarely, severe liver involvement requires surgery to reduce liver volume [55, 72]. In our adult model of *Pkd2* deletion, we found extensive liver cysts after six months, without detectable kidney cysts. Similarly, liver cysts were detected earlier than kidney cysts in an adult mouse model of Cre-mediated *Pkd1* deletion [52]. In our model, *Jnk* deletion suppressed hepatic cysts. A previous study demonstrated a requirement of *Jnk* for hepatic cyst formation in models of mitochondrial redox stress-induced cholangiocarcinoma [73]. However, this role of JNK to promote cystogenesis appears to be dependent on physiological context because *Jnk* deletion alone was sufficient to cause hepatic cyst formation in another study of aged mice [74-76]. JNK signaling may have tissue-specific roles in ADPKD that will be important to evaluate for therapeutic development.

Our work demonstrates that Pkd2 loss activates JNK and genetic removal of Jnk reduces cystic burden in mice with Pkd2 mutations. Further studies will elucidate the pathway by which

369 polycystin loss leads to JNK dysregulation, but our work suggests that JNK pathway inhibitors
370 could be effective treatments for ADPKD.

371 **Author Contributions**

372 GJP, RJD and AOS designed the experiments and co-wrote the manuscript; AOS, KMP and JAJ
373 performed experiments; AOS produced the figures.

374 **Acknowledgements**

375 This work was supported by National Institute of Health grant DK103632 to G.J.P and DK107220
376 to R.J.D. We thank Dr. Ichigo for providing *Ask1*$^{-/-}$ mice.

377 **Disclosures**

378 The authors have no conflicts to disclose.

379 **Supplemental Material Table of Contents**

390 **Figures**

391

Figure 1. Postnatal deletion of Pkd2 activates JNK signaling in mouse kidneys.

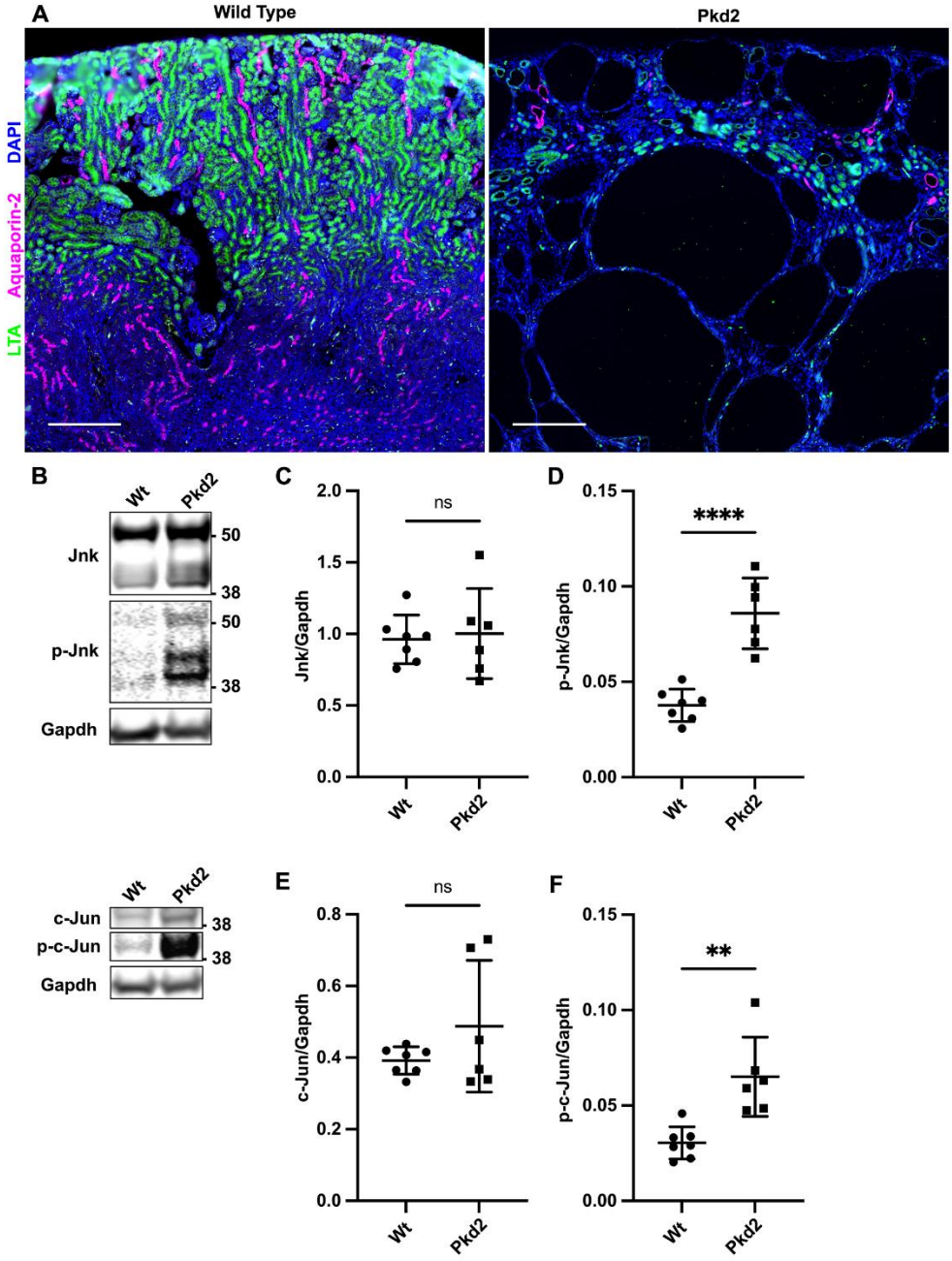

392

393

Figure 1. Postnatal deletion of *Pkd2* activates JNK signaling in juvenile mouse kidneys.

Mice with the following genotypes were treated with tamoxifen at P2-4 and collected at P21: Wt (*Rosa26-Cre^{ERT2}; Pkd2$^{fl/+}$*), Pkd2 (*Rosa26-Cre^{ERT2}; Pkd2$^{fl/fl}$*).

(A) Kidney sections were probed for tubule epithelial markers LTA (proximal tubules) and aquaporin-2 (collecting ducts). Nuclei were marked by DAPI. Images are slide scans obtained on Zeiss Axio Scan.Z1 with 20X objective. Scale bar is 500 microns.

(B) Whole kidney protein samples were immunoblotted for total Jnk, phospho T183/Y185 Jnk, total c-Jun, phospho S63 c-Jun, and loading control Gapdh.

(C-F) Quantification of immunoblots described in (B). N is 7 (Wt), 6 (Pkd2). ****, $P < 0.0001$; **, $P < 0.01$; ns, not significant by unpaired two-tailed t-test. Error bars indicate SD.

Figure 2. JNK inhibition reduces kidney cysts in juvenile Pkd2 mutant mice.

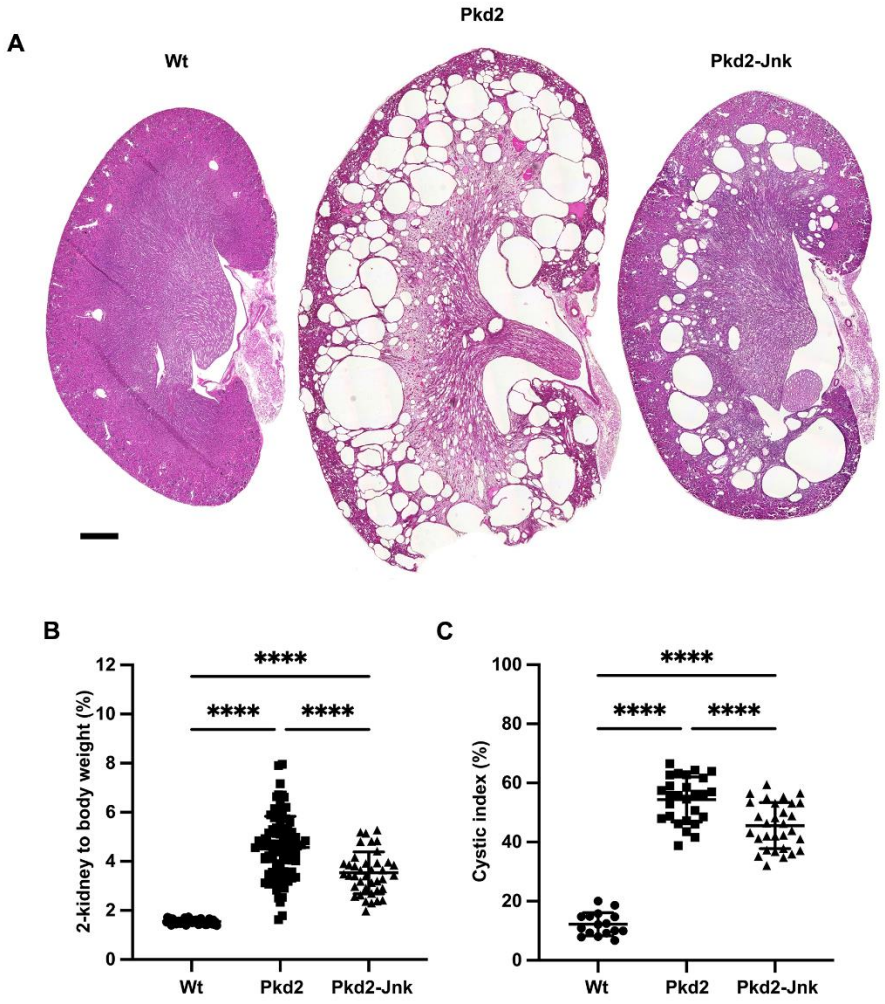

405

Figure 2. JNK inhibition reduces kidney cysts in juvenile *Pkd2* mutant mice.

Mice with the following genotypes were treated with tamoxifen at P2-4 and collected at P21: Wt (*Rosa26-Cre^{ERT2}; Pkd2$^{fl/+}$*), Pkd2 (*Rosa26-Cre^{ERT2}; Pkd2$^{fl/fl}$; Jnk1$^{+/+,\ fl/+}$; Jnk2$^{+/+,\ +/-}$*), and Pkd2-Jnk (*Rosa26-Cre^{ERT2}; Pkd2$^{fl/fl}$; Jnk1$^{fl/fl}$; Jnk2$^{null/null}$*).

(A) Kidney sections from P21 mice were stained with H&E to show the extent of disrupted organ architecture. Scale bar is 500 microns and applies to all images in the panel.

(B) Cystic burden was quantified using the ratio of 2-kidney weight / body weight x 100%. N is 42 (Wt), 88 (Pkd2), 39 (Pkd2-Jnk). ****, $P < 0.0001$ by one-way ANOVA followed by Tukey multiple comparison test with multiplicity-adjusted p-values. Error bars indicate SD.

(C) Cystic index (cystic area / total kidney area x 100%) was calculated for mid-sagittal H&E-stained kidney sections. N is 16 (Wt), 27 (Pkd2), 30 (Pkd2-Jnk). ****, $P < 0.0001$ by one-way ANOVA followed by Tukey multiple comparison test with multiplicity-adjusted p-values. Error bars indicate SD.

Figure 3. Pkd2 deletion activates c-Jun in kidney tubule epithelial cells.

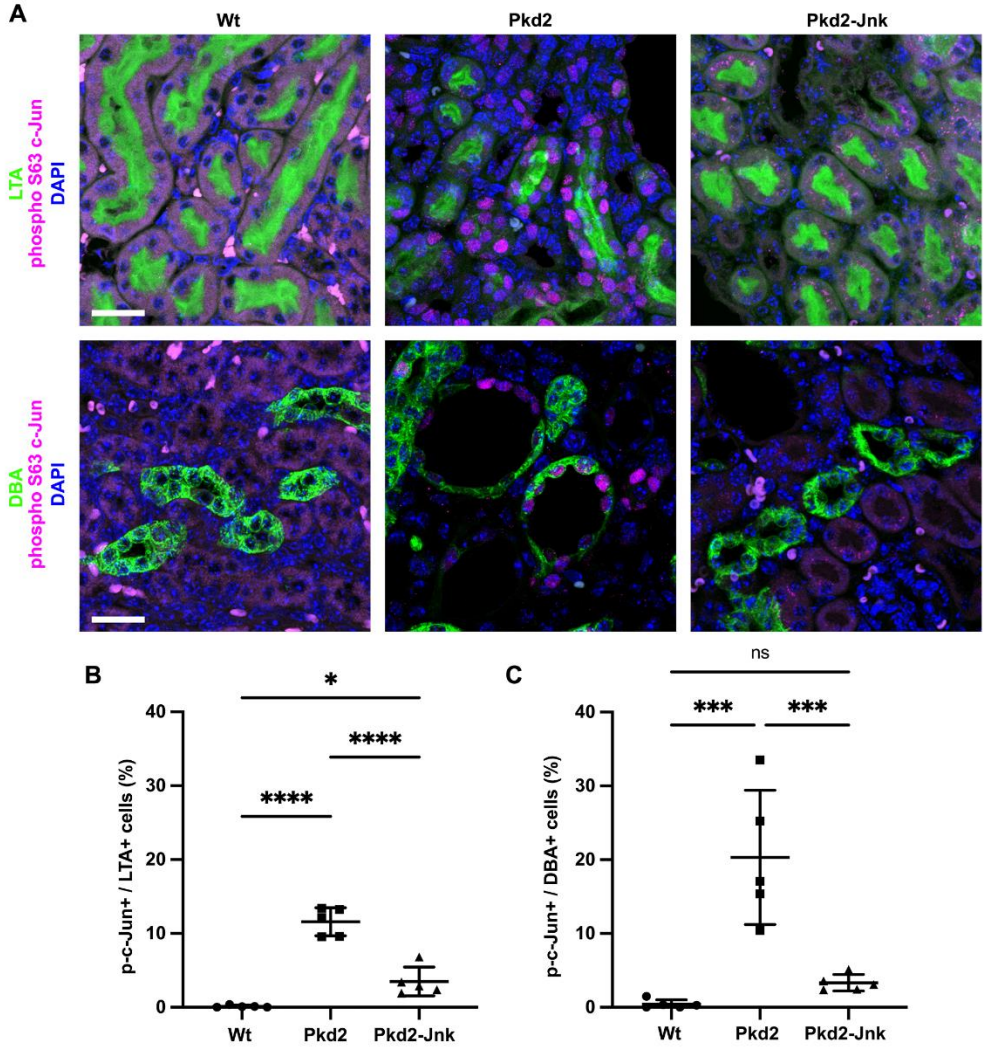

420

Figure 3. *Pkd2* deletion activates c-Jun in kidney tubule epithelial cells.

Mice with the following genotypes were treated with tamoxifen at P2-4 and collected at P21: Wt (*Rosa26-Cre^{ERT2}; Pkd2$^{fl/+}$*), Pkd2 (*Rosa26-Cre^{ERT2}; Pkd2$^{fl/fl}$; Jnk1$^{+/+,\ fl/+}$; Jnk2$^{+/+,\ +/-}$*), and Pkd2-Jnk (*Rosa26-Cre^{ERT2}; Pkd2$^{fl/fl}$; Jnk1$^{fl/fl}$; Jnk2$^{null/null}$*).

(A) Kidney sections were probed for phospho S63 c-Jun and tubule epithelial markers LTA (proximal tubules) or DBA (collecting ducts). Nuclei were marked by DAPI. Images are maximum projection of z-stacks (20 slices at 0.5um intervals) obtained on Zeiss LSM 900 Airyscan microscope with 40X objective. Scale bar is 20 microns and applies to all images in the panel.

(B-C) Quantification of the proportion of tubule epithelial cells with nuclei positive for phospho S63 c-Jun. (B) Proximal tubules (LTA+) and (C) collecting ducts (DBA+) were quantified separately. N is 5 animals per group, 1000-2000 cells per animal. ****, $P < 0.0001$; ***, $P < 0.001$; *, $P < 0.05$; ns, not significant by one-way ANOVA followed by Tukey multiple comparison test with multiplicity-adjusted p-values. Error bars indicate SD.

Figure 4. JNK inhibition reduces tubule cell proliferation in Pkd2 mutant mice.

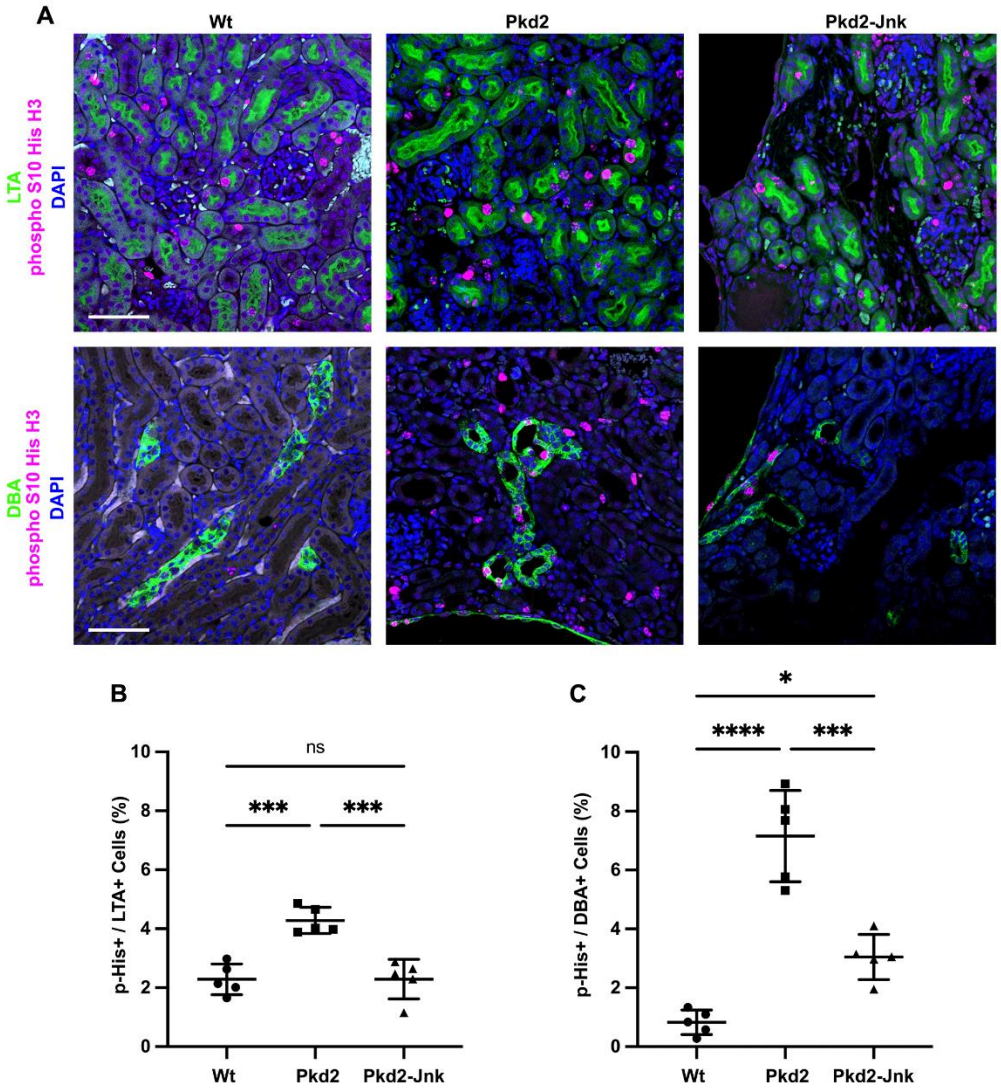

435

Figure 4. JNK inhibition reduces tubule cell proliferation in juvenile *Pkd2* mutant mice.

Mice with the following genotypes were treated with tamoxifen at P2-4 and collected at P21: Wt (*Rosa26-Cre^{ERT2}; Pkd2$^{fl/+}$*), Pkd2 (*Rosa26-Cre^{ERT2}; Pkd2$^{fl/fl}$; Jnk1$^{+/+,\ fl/+}$; Jnk2$^{+/+,\ +/-}$*), and Pkd2-Jnk (*Rosa26-Cre^{ERT2}; Pkd2$^{fl/fl}$; Jnk1$^{fl/fl}$; Jnk2$^{null/null}$*).

(A) Kidney sections from P21 mice were probed for the mitotic marker phospho S10 histone H3 along with tubule epithelial markers LTA (proximal tubules) and DBA (collecting ducts). Nuclei were marked with DAPI. Images are maximum projection of z-stacks (10 slices at 0.5um intervals) obtained on Zeiss LSM 900 Airyscan microscope with 20X objective. Scale bar is 50 microns and applies to all images in the panel.

(B-C) Quantification of the proportion of tubule cells with nuclei positive for phospho S10 histone H3. (B) Proximal tubule cells (LTA+) and (C) collecting duct cells (DBA+) were quantified separately. N is 5 animals per group, 1000-2000 cells per animal. ****, $P < 0.0001$; ***, $P < 0.001$; *, $P < 0.05$; ns, not significant by one-way ANOVA followed by Tukey multiple comparison test with multiplicity-adjusted p-values. Error bars indicate SD.

Figure 5. JNK inhibition reduces fibrosis in juvenile Pkd2 mutant mice.

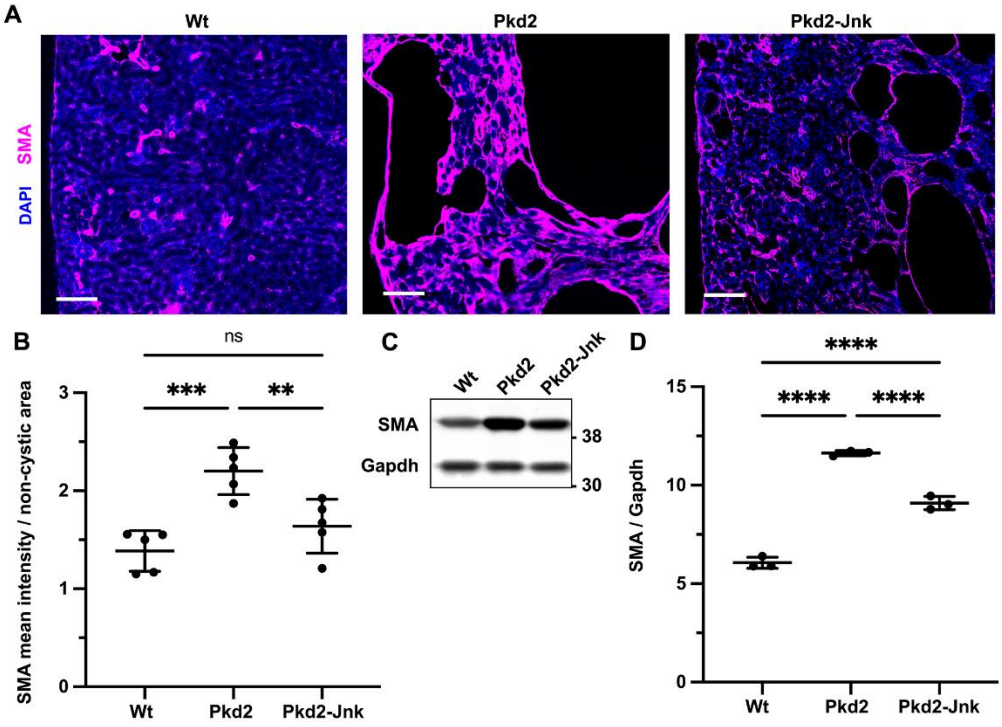

451

Figure 5. JNK inhibition reduces fibrosis in juvenile *Pkd2* mutant mice.

Mice with the following genotypes were treated with tamoxifen at P2-4 and collected at P21: Wt (*Rosa26-Cre^{ERT2}; Pkd2$^{fl/+}$*), Pkd2 (*Rosa26-Cre^{ERT2}; Pkd2$^{fl/fl}$; Jnk1$^{+/+,\ fl/+}$; Jnk2$^{+/+,\ +/-}$*), and Pkd2-Jnk (*Rosa26-Cre^{ERT2}; Pkd2$^{fl/fl}$; Jnk1$^{fl/fl}$; Jnk2$^{null/null}$*).

(A) Kidney sections from P21 mice were probed for SMA, a marker of active fibroblasts. Nuclei were stained with DAPI. Images are slide scans obtained on Zeiss Axio Scan.Z1 with 20X objective. Scale bar is 100 microns.

(B) Mean intensity of SMA staining and non-cystic kidney area were measured using ImageJ software. Graphed values are SMA mean intensity / non-cystic area * 100,000. N is 5 animals per group. ***, P< 0.001; **, P < 0.01; ns, not significant by one-way ANOVA followed by Tukey multiple comparison test with multiplicity-adjusted p-values. Error bars indicate SD.

(C) Whole kidney protein samples from P21 mice were immunoblotted for SMA and loading control Gapdh.

(D) Quantification of immunoblots described in (C). N is 3 animals per groups. ****, P < 0.0001 by one-way ANOVA followed by Tukey multiple comparison test with multiplicity-adjusted p-values. Error bars indicate SD.

Figure 6. Jnk1 deletion is primarily responsible for reduction in cystic phenotype in Pkd2 mutant mice.

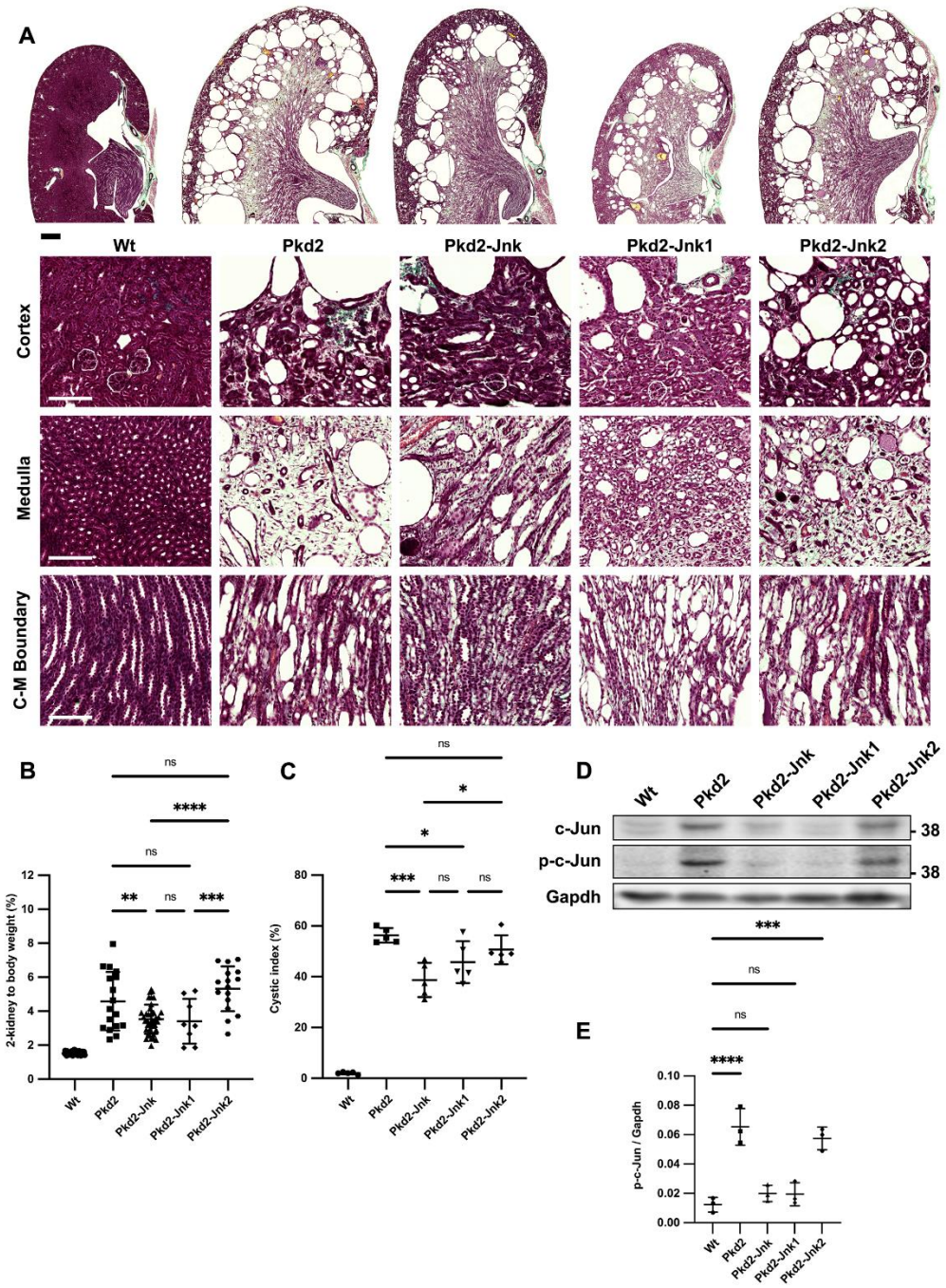

Figure 6. *Jnk1* deletion rather than *Jnk2* is primarily responsible for reducing cystic disease in juvenile *Pkd2* mutant kidneys.

Mice with the following genotypes were treated with tamoxifen at P2-4 and collected at P21: Pkd2-Jnk1 (*Rosa26-Cre^{ERT2}; Pkd2$^{fl/fl}$; Jnk1$^{null/null}$; Jnk2$^{+/+}$*); Pkd2-Jnk2 (*Rosa26-Cre^{ERT2}; Pkd2$^{fl/fl}$; JNK1$^{+/+}$; Jnk2$^{null/null}$*). We compared the results from these animals to the groups described previously: Wt (*Rosa26-Cre^{ERT2}; Pkd2$^{fl/+}$, JNK1$^{+/+}$; Jnk2$^{+/+}$*), Pkd2 (*Rosa26-Cre^{ERT2}; Pkd2$^{fl/fl}$; JNK1$^{+/+}$; Jnk2$^{+/+}$*), Pkd2-Jnk (*Rosa26-Cre^{ERT2}; Pkd2$^{fl/fl}$; Jnk1$^{fl/fl}$; Jnk2$^{null/null}$*).

(A) Kidney sections were stained with one-step trichrome which marks collagen fibers pale green, cytoplasm red, and nuclei dark blue. Scale bar for full size kidney scans is 500 microns. Insets show detail from cortex (top), cortical-medullary boundary (middle), and medulla (bottom). Scale bar for insets is 100 microns.

(B) Cystic burden was quantified using the ratio of 2-kidney weight / body weight x 100%. Wt and Pkd2-Jnk data is the same as shown in Figure 2B. Pkd2 data overlaps with Figure 2B, but only includes animals with four wild-type alleles of Jnk. N is 42 (Wt), 17 (Pkd2), 39 (Pkd2-Jnk), 8 (Pkd2-Jnk1), 16 (Pkd2-Jnk2). ****, $P < 0.0001$; ***, $P < 0.001$; **, $P < 0.01$; ns, not significant by one-way ANOVA followed by Tukey multiple comparison test with multiplicity-adjusted p-values. Error bars indicate SD.

(C) Cystic index (cystic area / total kidney area * 100%) was calculated for mid-sagittal trichrome-stained kidney sections. N is 5 animals per group. ***, $P < 0.001$; *, $P < 0.05$; ns, not significant by one-way ANOVA followed by Tukey multiple comparison test with multiplicity-adjusted p-values. Error bars indicate SD.

(D) Whole kidney protein lysates were immunoblotted for total c-Jun, phospho S63 c-Jun and loading control Gapdh.

(E) Quantification of immunoblots described in (D). N is 3 animals per group. ****, $P < 0.0001$; ***, $P < 0.001$; ns, not significant by one-way ANOVA followed by Tukey multiple comparison test with multiplicity-adjusted p-values. Error bars indicate SD.

Figure 7. JNK inhibition reduces cysts in adult Pkd2 mutant livers.

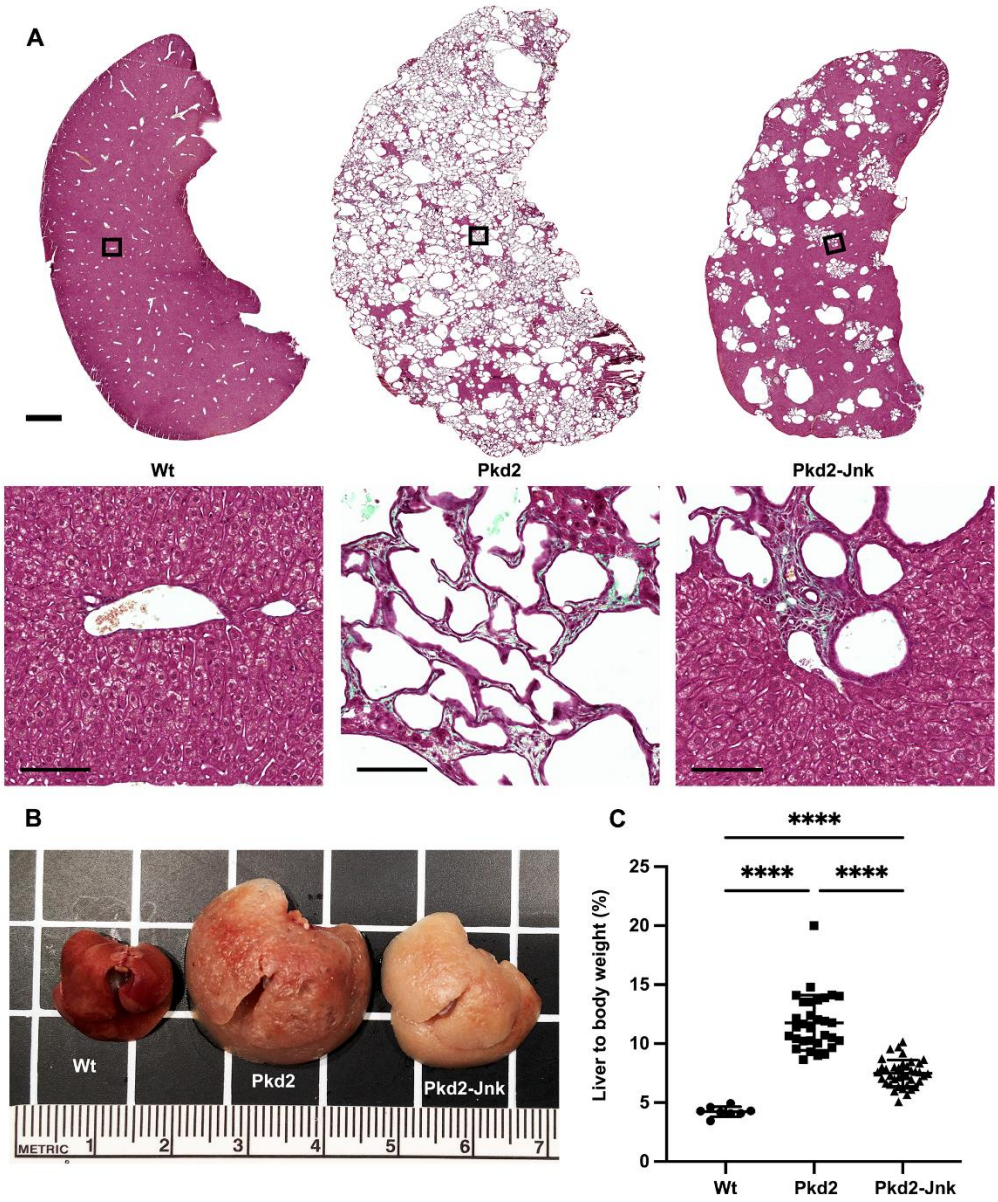

497

Figure 7. JNK inhibition reduces cysts in in adult *Pkd2* mutant livers.

Mice with the following genotypes were treated with tamoxifen at P21-23 and collected 24 weeks later: Wt (*Rosa26-Cre^{ERT2}; Pkd2$^{fl/+}$*), Pkd2 (*Rosa26-Cre^{ERT2}; Pkd2$^{fl/fl}$; Jnk1$^{+/+,\ fl/+}$; Jnk2$^{+/+,\ +/-}$*), Pkd2-Jnk (*Rosa26-Cre^{ERT2}; Pkd2$^{fl/fl}$; Jnk1$^{fl/fl}$; Jnk2$^{null/null}$*).

(A) Liver sections were stained with one-step trichrome to mark collagen fibers pale green, cytoplasm red, and nuclei dark blue. Black boxes indicate magnified regions. Scale bar is 1000 microns for full size liver scans, 100 microns for insets.

(B) Gross morphology of cystic livers. Centimeter ruler is shown.

(C) Cystic burden in the liver was quantified using the ratio of liver weight / body weight x 100%. N is 8 (Wt), 31 (Pkd2), 38 (Pkd2-Jnk). ****, $P < 0.0001$; ***, $P < 0.001$ by one-way ANOVA followed by Tukey multiple comparison test with multiplicity-adjusted p-values. Error bars indicate SD.

References

1. Su Q, Hu F, Ge X, Lei J, Yu S, Wang T, et al. Structure of the human PKD1-PKD2 complex. Science. 2018;361(6406). Epub 2018/08/11. doi: 10.1126/science.aat9819. PubMed PMID: 30093605.

2. Pazour GJ. Intraflagellar transport and cilia-dependent renal disease: the ciliary hypothesis of polycystic kidney disease. J Am Soc Nephrol. 2004;15(10):2528-36. Epub 2004/10/07. doi: 10.1097/01.ASN.0000141055.57643.E0. PubMed PMID: 15466257.

3. Ma M, Tian X, Igarashi P, Pazour GJ, Somlo S. Loss of cilia suppresses cyst growth in genetic models of autosomal dominant polycystic kidney disease. Nat Genet. 2013;45(9):1004-12. Epub 2013/07/31. doi: 10.1038/ng.2715. PubMed PMID: 23892607; PubMed Central PMCID: PMCPMC3758452.

4. Ma M, Gallagher AR, Somlo S. Ciliary Mechanisms of Cyst Formation in Polycystic Kidney Disease. Cold Spring Harb Perspect Biol. 2017;9(11). Epub 2017/03/23. doi: 10.1101/cshperspect.a028209. PubMed PMID: 28320755; PubMed Central PMCID: PMCPMC5666631.

5. Yamaguchi T, Hempson SJ, Reif GA, Hedge AM, Wallace DP. Calcium restores a normal proliferation phenotype in human polycystic kidney disease epithelial cells. J Am Soc Nephrol. 2006;17(1):178-87. Epub 2005/12/02. doi: 10.1681/ASN.2005060645. PubMed PMID: 16319189.

6. Yamaguchi T, Wallace DP, Magenheimer BS, Hempson SJ, Grantham JJ, Calvet JP. Calcium restriction allows cAMP activation of the B-Raf/ERK pathway, switching cells to a cAMP-dependent growth-stimulated phenotype. J Biol Chem. 2004;279(39):40419-30. Epub 2004/07/21. doi: 10.1074/jbc.M405079200. PubMed PMID: 15263001.

7. Calvet JP. The Role of Calcium and Cyclic AMP in PKD. In: Li X, editor. Polycystic Kidney Disease. Brisbane (AU)2015.
8. Belibi FA, Reif G, Wallace DP, Yamaguchi T, Olsen L, Li H, et al. Cyclic AMP promotes growth and secretion in human polycystic kidney epithelial cells. Kidney Int. 2004;66(3):964-73. Epub 2004/08/26. doi: 10.1111/j.1523-1755.2004.00843.x. PubMed PMID: 15327388.
9. Torres VE, Higashihara E, Devuyst O, Chapman AB, Gansevoort RT, Grantham JJ, et al. Effect of Tolvaptan in Autosomal Dominant Polycystic Kidney Disease by CKD Stage: Results from the TEMPO 3:4 Trial. Clin J Am Soc Nephrol. 2016;11(5):803-11. Epub 2016/02/26. doi: 10.2215/CJN.06300615. PubMed PMID: 26912543; PubMed Central PMCID: PMCPMC4858477.
10. Torres VE, Chapman AB, Devuyst O, Gansevoort RT, Perrone RD, Koch G, et al. Tolvaptan in Later-Stage Autosomal Dominant Polycystic Kidney Disease. N Engl J Med. 2017;377(20):1930-42. Epub 2017/11/07. doi: 10.1056/NEJMoa1710030. PubMed PMID: 29105594.
11. Chebib FT, Perrone RD, Chapman AB, Dahl NK, Harris PC, Mrug M, et al. A Practical Guide for Treatment of Rapidly Progressive ADPKD with Tolvaptan. J Am Soc Nephrol. 2018;29(10):2458-70. Epub 2018/09/20. doi: 10.1681/ASN.2018060590. PubMed PMID: 30228150; PubMed Central PMCID: PMCPMC6171265.
12. Arnould T, Kim E, Tsiokas L, Jochimsen F, Gruning W, Chang JD, et al. The polycystic kidney disease 1 gene product mediates protein kinase C alpha-dependent and c-Jun N-terminal kinase-dependent activation of the transcription factor AP-1. J Biol Chem. 1998;273(11):6013-8. Epub 1998/04/16. PubMed PMID: 9497315.
13. Parnell SC, Magenheimer BS, Maser RL, Zien CA, Frischauf AM, Calvet JP. Polycystin-1 activation of c-Jun N-terminal kinase and AP-1 is mediated by heterotrimeric G proteins. J Biol Chem. 2002;277(22):19566-72. Epub 2002/03/26. doi: 10.1074/jbc.M201875200. PubMed PMID: 11912216.
14. Arnould T, Sellin L, Benzing T, Tsiokas L, Cohen HT, Kim E, et al. Cellular activation triggered by the autosomal dominant polycystic kidney disease gene product PKD2. Mol Cell Biol. 1999;19(5):3423-34. Epub 1999/04/17. PubMed PMID: 10207066; PubMed Central PMCID: PMCPMC84135.
15. Yu W, Kong T, Beaudry S, Tran M, Negoro H, Yanamadala V, et al. Polycystin-1 protein level determines activity of the Galpha12/JNK apoptosis pathway. J Biol Chem. 2010;285(14):10243-51. Epub 2010/01/29. doi: 10.1074/jbc.M109.070821. PubMed PMID: 20106977; PubMed Central PMCID: PMCPMC2856229.
16. Le NH, van der Wal A, van der Bent P, Lantinga-van Leeuwen IS, Breuning MH, van Dam H, et al. Increased activity of activator protein-1 transcription factor components ATF2, c-Jun, and c-Fos in human and mouse autosomal dominant polycystic kidney disease. J Am Soc Nephrol. 2005;16(9):2724-31. Epub 2005/07/29. doi: 10.1681/ASN.2004110913. PubMed PMID: 16049073.
17. Nishio S, Hatano M, Nagata M, Horie S, Koike T, Tokuhisa T, et al. Pkd1 regulates immortalized proliferation of renal tubular epithelial cells through p53 induction and JNK activation. J Clin Invest. 2005;115(4):910-8. Epub 2005/03/12. doi: 10.1172/JCI22850. PubMed PMID: 15761494; PubMed Central PMCID: PMCPMC1059447.
18. Davis RJ. Signal transduction by the JNK group of MAP kinases. Cell. 2000;103(2):239-52. Epub 2000/11/01. doi: 10.1016/s0092-8674(00)00116-1. PubMed PMID: 11057897.

19. Smeal T, Binetruy B, Mercola DA, Birrer M, Karin M. Oncogenic and transcriptional cooperation with Ha-Ras requires phosphorylation of c-Jun on serines 63 and 73. Nature. 1991;354(6353):494-6. Epub 1991/12/12. doi: 10.1038/354494a0. PubMed PMID: 1749429.
20. Parrot C, Kurbegovic A, Yao G, Couillard M, Cote O, Trudel M. c-Myc is a regulator of the PKD1 gene and PC1-induced pathogenesis. Hum Mol Genet. 2019;28(5):751-63. Epub 2018/11/06. doi: 10.1093/hmg/ddy379. PubMed PMID: 30388220; PubMed Central PMCID: PMCPMC6381314.
21. Lee EJ, Seo E, Kim JW, Nam SA, Lee JY, Jun J, et al. TAZ/Wnt-beta-catenin/c-MYC axis regulates cystogenesis in polycystic kidney disease. Proc Natl Acad Sci U S A. 2020;117(46):29001-12. Epub 2020/10/31. doi: 10.1073/pnas.2009334117. PubMed PMID: 33122431.
22. De Borst MH, Prakash J, Melenhorst WB, van den Heuvel MC, Kok RJ, Navis G, et al. Glomerular and tubular induction of the transcription factor c-Jun in human renal disease. J Pathol. 2007;213(2):219-28. Epub 2007/09/25. doi: 10.1002/path.2228. PubMed PMID: 17891746.
23. Grynberg K, Ozols E, Mulley WR, Davis RJ, Flavell RA, Nikolic-Paterson DJ, et al. JNK1 signaling in the proximal tubule causes cell death and acute renal failure in rat and mouse models of renal ischaemia/reperfusion injury. Am J Pathol. 2021. Epub 2021/02/20. doi: 10.1016/j.ajpath.2021.02.004. PubMed PMID: 33607044.
24. Kanellis J, Ma FY, Kandane-Rathnayake R, Dowling JP, Polkinghorne KR, Bennett BL, et al. JNK signalling in human and experimental renal ischaemia/reperfusion injury. Nephrol Dial Transplant. 2010;25(9):2898-908. Epub 2010/04/07. doi: 10.1093/ndt/gfq147. PubMed PMID: 20368303.
25. Ma FY, Flanc RS, Tesch GH, Bennett BL, Friedman GC, Nikolic-Paterson DJ. Blockade of the c-Jun amino terminal kinase prevents crescent formation and halts established anti-GBM glomerulonephritis in the rat. Lab Invest. 2009;89(4):470-84. Epub 2009/02/04. doi: 10.1038/labinvest.2009.2. PubMed PMID: 19188913.
26. Ma FY, Flanc RS, Tesch GH, Han Y, Atkins RC, Bennett BL, et al. A pathogenic role for c-Jun amino-terminal kinase signaling in renal fibrosis and tubular cell apoptosis. J Am Soc Nephrol. 2007;18(2):472-84. Epub 2007/01/05. doi: 10.1681/ASN.2006060604. PubMed PMID: 17202416.
27. de Borst MH, Prakash J, Sandovici M, Klok PA, Hamming I, Kok RJ, et al. c-Jun NH2-terminal kinase is crucially involved in renal tubulo-interstitial inflammation. J Pharmacol Exp Ther. 2009;331(3):896-905. Epub 2009/09/01. doi: 10.1124/jpet.109.154179. PubMed PMID: 19717791.
28. Happe H, Leonhard WN, van der Wal A, van de Water B, Lantinga-van Leeuwen IS, Breuning MH, et al. Toxic tubular injury in kidneys from Pkd1-deletion mice accelerates cystogenesis accompanied by dysregulated planar cell polarity and canonical Wnt signaling pathways. Hum Mol Genet. 2009;18(14):2532-42. Epub 2009/04/30. doi: 10.1093/hmg/ddp190. PubMed PMID: 19401297.
29. Prasad S, McDaid JP, Tam FW, Haylor JL, Ong AC. Pkd2 dosage influences cellular repair responses following ischemia-reperfusion injury. Am J Pathol. 2009;175(4):1493-503. Epub 2009/09/05. doi: 10.2353/ajpath.2009.090227. PubMed PMID: 19729489; PubMed Central PMCID: PMCPMC2751546.

30. Kurbegovic A, Trudel M. Acute kidney injury induces hallmarks of polycystic kidney disease. Am J Physiol Renal Physiol. 2016;311(4):F740-F51. Epub 2016/08/05. doi: 10.1152/ajprenal.00167.2016. PubMed PMID: 27488998.
31. Wernig G, Chen SY, Cui L, Van Neste C, Tsai JM, Kambham N, et al. Unifying mechanism for different fibrotic diseases. Proc Natl Acad Sci U S A. 2017;114(18):4757-62. Epub 2017/04/21. doi: 10.1073/pnas.1621375114. PubMed PMID: 28424250; PubMed Central PMCID: PMCPMC5422830.
32. Garcia-Gonzalez MA, Outeda P, Zhou Q, Zhou F, Menezes LF, Qian F, et al. Pkd1 and Pkd2 are required for normal placental development. PLoS One. 2010;5(9). Epub 2010/09/24. doi: 10.1371/journal.pone.0012821. PubMed PMID: 20862291; PubMed Central PMCID: PMCPMC2940908.
33. Das M, Jiang F, Sluss HK, Zhang C, Shokat KM, Flavell RA, et al. Suppression of p53-dependent senescence by the JNK signal transduction pathway. Proc Natl Acad Sci U S A. 2007;104(40):15759-64. Epub 2007/09/26. doi: 10.1073/pnas.0707782104. PubMed PMID: 17893331; PubMed Central PMCID: PMCPMC2000443.
34. Yang DD, Conze D, Whitmarsh AJ, Barrett T, Davis RJ, Rincon M, et al. Differentiation of CD4+ T cells to Th1 cells requires MAP kinase JNK2. Immunity. 1998;9(4):575-85. Epub 1998/11/07. doi: 10.1016/s1074-7613(00)80640-8. PubMed PMID: 9806643.
35. Badea TC, Wang Y, Nathans J. A noninvasive genetic/pharmacologic strategy for visualizing cell morphology and clonal relationships in the mouse. J Neurosci. 2003;23(6):2314-22. Epub 2003/03/27. PubMed PMID: 12657690; PubMed Central PMCID: PMCPMC6742025.
36. Tobiume K, Matsuzawa A, Takahashi T, Nishitoh H, Morita K, Takeda K, et al. ASK1 is required for sustained activations of JNK/p38 MAP kinases and apoptosis. EMBO Rep. 2001;2(3):222-8. Epub 2001/03/27. doi: 10.1093/embo-reports/kve046. PubMed PMID: 11266364; PubMed Central PMCID: PMCPMC1083842.
37. Kant S, Swat W, Zhang S, Zhang ZY, Neel BG, Flavell RA, et al. TNF-stimulated MAP kinase activation mediated by a Rho family GTPase signaling pathway. Genes Dev. 2011;25(19):2069-78. Epub 2011/10/08. doi: 10.1101/gad.17224711. PubMed PMID: 21979919; PubMed Central PMCID: PMCPMC3197205.
38. Brancho D, Ventura JJ, Jaeschke A, Doran B, Flavell RA, Davis RJ. Role of MLK3 in the regulation of mitogen-activated protein kinase signaling cascades. Mol Cell Biol. 2005;25(9):3670-81. Epub 2005/04/16. doi: 10.1128/MCB.25.9.3670-3681.2005. PubMed PMID: 15831472; PubMed Central PMCID: PMCPMC1084312.
39. Sadate-Ngatchou PI, Payne CJ, Dearth AT, Braun RE. Cre recombinase activity specific to postnatal, premeiotic male germ cells in transgenic mice. Genesis. 2008;46(12):738-42. Epub 2008/10/14. doi: 10.1002/dvg.20437. PubMed PMID: 18850594; PubMed Central PMCID: PMCPMC2837914.
40. Ventura A, Kirsch DG, McLaughlin ME, Tuveson DA, Grimm J, Lintault L, et al. Restoration of p53 function leads to tumour regression in vivo. Nature. 2007;445(7128):661-5. Epub 2007/01/26. doi: 10.1038/nature05541. PubMed PMID: 17251932.
41. Chang-Panesso M, Kadyrov FF, Machado FG, Kumar A, Humphreys BD. Meis1 is specifically upregulated in kidney myofibroblasts during aging and injury but is not required for kidney homeostasis or fibrotic response. Am J Physiol Renal Physiol. 2018;315(2):F275-F90.

664 Epub 2018/03/30. doi: 10.1152/ajprenal.00030.2018. PubMed PMID: 29592525; PubMed
665 Central PMCID: PMCPMC6139520.
666 42. Tesch GH, Ma FY, Nikolic-Paterson DJ. Targeting apoptosis signal-regulating kinase 1 in
667 acute and chronic kidney disease. Anat Rec (Hoboken). 2020. Epub 2020/01/24. doi:
668 10.1002/ar.24373. PubMed PMID: 31971352.
669 43. Teramoto H, Coso OA, Miyata H, Igishi T, Miki T, Gutkind JS. Signaling from the small
670 GTP-binding proteins Rac1 and Cdc42 to the c-Jun N-terminal kinase/stress-activated protein
671 kinase pathway. A role for mixed lineage kinase 3/protein-tyrosine kinase 1, a novel member of
672 the mixed lineage kinase family. J Biol Chem. 1996;271(44):27225-8. Epub 1996/11/01. doi:
673 10.1074/jbc.271.44.27225. PubMed PMID: 8910292.
674 44. Du Y, Bock BC, Schachter KA, Chao M, Gallo KA. Cdc42 induces activation loop
675 phosphorylation and membrane targeting of mixed lineage kinase 3. J Biol Chem.
676 2005;280(52):42984-93. Epub 2005/10/29. doi: 10.1074/jbc.M502671200. PubMed PMID:
677 16253996.
678 45. Pulverer BJ, Kyriakis JM, Avruch J, Nikolakaki E, Woodgett JR. Phosphorylation of c-jun
679 mediated by MAP kinases. Nature. 1991;353(6345):670-4. Epub 1991/10/17. doi:
680 10.1038/353670a0. PubMed PMID: 1922387.
681 46. Zhang C, Balbo B, Ma M, Zhao J, Tian X, Kluger Y, et al. Cyclin-Dependent Kinase 1
682 Activity Is a Driver of Cyst Growth in Polycystic Kidney Disease. J Am Soc Nephrol. 2020. Epub
683 2020/10/14. doi: 10.1681/ASN.2020040511. PubMed PMID: 33046531.
684 47. Zhang Y, Dai Y, Raman A, Daniel E, Metcalf J, Reif G, et al. Overexpression of TGF-beta1
685 induces renal fibrosis and accelerates the decline in kidney function in polycystic kidney
686 disease. Am J Physiol Renal Physiol. 2020;319(6):F1135-F48. Epub 2020/11/10. doi:
687 10.1152/ajprenal.00366.2020. PubMed PMID: 33166182.
688 48. Wu Q, Wu W, Jacevic V, Franca TCC, Wang X, Kuca K. Selective inhibitors for JNK
689 signalling: a potential targeted therapy in cancer. J Enzyme Inhib Med Chem. 2020;35(1):574-
690 83. Epub 2020/01/30. doi: 10.1080/14756366.2020.1720013. PubMed PMID: 31994958;
691 PubMed Central PMCID: PMCPMC7034130.
692 49. Manning AM, Davis RJ. Targeting JNK for therapeutic benefit: from junk to gold? Nat Rev
693 Drug Discov. 2003;2(7):554-65. Epub 2003/06/20. doi: 10.1038/nrd1132. PubMed PMID:
694 12815381.
695 50. Gupta S, Barrett T, Whitmarsh AJ, Cavanagh J, Sluss HK, Derijard B, et al. Selective
696 interaction of JNK protein kinase isoforms with transcription factors. EMBO J.
697 1996;15(11):2760-70. Epub 1996/06/03. PubMed PMID: 8654373; PubMed Central PMCID:
698 PMCPMC450211.
699 51. Derijard B, Hibi M, Wu IH, Barrett T, Su B, Deng T, et al. JNK1: a protein kinase
700 stimulated by UV light and Ha-Ras that binds and phosphorylates the c-Jun activation domain.
701 Cell. 1994;76(6):1025-37. Epub 1994/03/25. doi: 10.1016/0092-8674(94)90380-8. PubMed
702 PMID: 8137421.
703 52. Piontek K, Menezes LF, Garcia-Gonzalez MA, Huso DL, Germino GG. A critical
704 developmental switch defines the kinetics of kidney cyst formation after loss of Pkd1. Nat Med.
705 2007;13(12):1490-5. Epub 2007/10/30. doi: 10.1038/nm1675. PubMed PMID: 17965720;
706 PubMed Central PMCID: PMCPMC2302790.

53. Lantinga-van Leeuwen IS, Leonhard WN, van der Wal A, Breuning MH, de Heer E, Peters DJ. Kidney-specific inactivation of the Pkd1 gene induces rapid cyst formation in developing kidneys and a slow onset of disease in adult mice. Hum Mol Genet. 2007;16(24):3188-96. Epub 2007/10/13. doi: 10.1093/hmg/ddm299. PubMed PMID: 17932118.
54. Everson GT. Hepatic cysts in autosomal dominant polycystic kidney disease. Am J Kidney Dis. 1993;22(4):520-5. Epub 1993/10/01. doi: 10.1016/s0272-6386(12)80923-1. PubMed PMID: 8213790.
55. Chauveau D, Fakhouri F, Grunfeld JP. Liver involvement in autosomal-dominant polycystic kidney disease: therapeutic dilemma. J Am Soc Nephrol. 2000;11(9):1767-75. Epub 2000/08/31. PubMed PMID: 10966503.
56. Lim AK, Ma FY, Nikolic-Paterson DJ, Ozols E, Young MJ, Bennett BL, et al. Evaluation of JNK blockade as an early intervention treatment for type 1 diabetic nephropathy in hypertensive rats. Am J Nephrol. 2011;34(4):337-46. Epub 2011/08/31. doi: 10.1159/000331058. PubMed PMID: 21876346.
57. Uehara T, Bennett B, Sakata ST, Satoh Y, Bilter GK, Westwick JK, et al. JNK mediates hepatic ischemia reperfusion injury. J Hepatol. 2005;42(6):850-9. Epub 2005/05/12. doi: 10.1016/j.jhep.2005.01.030. PubMed PMID: 15885356.
58. Uehara T, Xi Peng X, Bennett B, Satoh Y, Friedman G, Currin R, et al. c-Jun N-terminal kinase mediates hepatic injury after rat liver transplantation. Transplantation. 2004;78(3):324-32. Epub 2004/08/19. doi: 10.1097/01.tp.0000128859.42696.28. PubMed PMID: 15316358.
59. Bubici C, Papa S. JNK signalling in cancer: in need of new, smarter therapeutic targets. Br J Pharmacol. 2014;171(1):24-37. Epub 2013/10/15. doi: 10.1111/bph.12432. PubMed PMID: 24117156; PubMed Central PMCID: PMCPMC3874694.
60. Tomita K, Kohli R, MacLaurin BL, Hirsova P, Guo Q, Sanchez LHG, et al. Mixed-lineage kinase 3 pharmacological inhibition attenuates murine nonalcoholic steatohepatitis. JCI Insight. 2017;2(15). Epub 2017/08/05. doi: 10.1172/jci.insight.94488. PubMed PMID: 28768902; PubMed Central PMCID: PMCPMC5543922.
61. Dong W, Embury CM, Lu Y, Whitmire SM, Dyavarshetty B, Gelbard HA, et al. The mixed-lineage kinase 3 inhibitor URMC-099 facilitates microglial amyloid-beta degradation. J Neuroinflammation. 2016;13(1):184. Epub 2016/07/13. doi: 10.1186/s12974-016-0646-z. PubMed PMID: 27401058; PubMed Central PMCID: PMCPMC4940949.
62. Kiyota T, Machhi J, Lu Y, Dyavarshetty B, Nemati M, Zhang G, et al. URMC-099 facilitates amyloid-beta clearance in a murine model of Alzheimer's disease. J Neuroinflammation. 2018;15(1):137. Epub 2018/05/08. doi: 10.1186/s12974-018-1172-y. PubMed PMID: 29729668; PubMed Central PMCID: PMCPMC5935963.
63. Younossi ZM, Stepanova M, Lawitz E, Charlton M, Loomba R, Myers RP, et al. Improvement of hepatic fibrosis and patient-reported outcomes in non-alcoholic steatohepatitis treated with selonsertib. Liver Int. 2018;38(10):1849-59. Epub 2018/01/30. doi: 10.1111/liv.13706. PubMed PMID: 29377462.
64. Loomba R, Lawitz E, Mantry PS, Jayakumar S, Caldwell SH, Arnold H, et al. The ASK1 inhibitor selonsertib in patients with nonalcoholic steatohepatitis: A randomized, phase 2 trial. Hepatology. 2018;67(2):549-59. Epub 2017/09/12. doi: 10.1002/hep.29514. PubMed PMID: 28892558; PubMed Central PMCID: PMCPMC5814892.

65. Weston CR, Davis RJ. The JNK signal transduction pathway. Curr Opin Cell Biol. 2007;19(2):142-9. Epub 2007/02/17. doi: 10.1016/j.ceb.2007.02.001. PubMed PMID: 17303404.
66. Parnell SC, Magenheimer BS, Maser RL, Pavlov TS, Havens MA, Hastings ML, et al. A mutation affecting polycystin-1 mediated heterotrimeric G-protein signaling causes PKD. Hum Mol Genet. 2018;27(19):3313-24. Epub 2018/06/23. doi: 10.1093/hmg/ddy223. PubMed PMID: 29931260; PubMed Central PMCID: PMCPMC6140781.
67. Zhao HF, Wang J, Tony To SS. The phosphatidylinositol 3-kinase/Akt and c-Jun N-terminal kinase signaling in cancer: Alliance or contradiction? (Review). Int J Oncol. 2015;47(2):429-36. Epub 2015/06/18. doi: 10.3892/ijo.2015.3052. PubMed PMID: 26082006.
68. Wu Q, Wu W, Fu B, Shi L, Wang X, Kuca K. JNK signaling in cancer cell survival. Med Res Rev. 2019;39(6):2082-104. Epub 2019/03/27. doi: 10.1002/med.21574. PubMed PMID: 30912203.
69. Abdelrahman KS, Hassan HA, Abdel-Aziz SA, Marzouk AA, Narumi A, Konno H, et al. JNK signaling as a target for anticancer therapy. Pharmacol Rep. 2021;73(2):405-34. Epub 2021/03/13. doi: 10.1007/s43440-021-00238-y. PubMed PMID: 33710509.
70. Vernia S, Edwards YJ, Han MS, Cavanagh-Kyros J, Barrett T, Kim JK, et al. An alternative splicing program promotes adipose tissue thermogenesis. Elife. 2016;5. Epub 2016/09/17. doi: 10.7554/eLife.17672. PubMed PMID: 27635635; PubMed Central PMCID: PMCPMC5026472.
71. Bae KT, Zhu F, Chapman AB, Torres VE, Grantham JJ, Guay-Woodford LM, et al. Magnetic resonance imaging evaluation of hepatic cysts in early autosomal-dominant polycystic kidney disease: the Consortium for Radiologic Imaging Studies of Polycystic Kidney Disease cohort. Clin J Am Soc Nephrol. 2006;1(1):64-9. Epub 2007/08/21. doi: 10.2215/CJN.00080605. PubMed PMID: 17699192.
72. Gevers TJ, Chrispijn M, Wetzels JF, Drenth JP. Rationale and design of the RESOLVE trial: lanreotide as a volume reducing treatment for polycystic livers in patients with autosomal dominant polycystic kidney disease. BMC Nephrol. 2012;13:17. Epub 2012/04/06. doi: 10.1186/1471-2369-13-17. PubMed PMID: 22475206; PubMed Central PMCID: PMCPMC3368739.
73. Yuan D, Huang S, Berger E, Liu L, Gross N, Heinzmann F, et al. Kupffer Cell-Derived Tnf Triggers Cholangiocellular Tumorigenesis through JNK due to Chronic Mitochondrial Dysfunction and ROS. Cancer Cell. 2017;31(6):771-89 e6. Epub 2017/06/14. doi: 10.1016/j.ccell.2017.05.006. PubMed PMID: 28609656; PubMed Central PMCID: PMCPMC7909318.
74. Cubero FJ, Mohamed MR, Woitok MM, Zhao G, Hatting M, Nevzorova YA, et al. Loss of c-Jun N-terminal Kinase 1 and 2 Function in Liver Epithelial Cells Triggers Biliary Hyperproliferation Resembling Cholangiocarcinoma. Hepatol Commun. 2020;4(6):834-51. Epub 2020/06/04. doi: 10.1002/hep4.1495. PubMed PMID: 32490320; PubMed Central PMCID: PMCPMC7262317.
75. Muller K, Honcharova-Biletska H, Koppe C, Egger M, Chan LK, Schneider AT, et al. JNK signaling prevents biliary cyst formation through a CASPASE-8-dependent function of RIPK1 during aging. Proc Natl Acad Sci U S A. 2021;118(12). Epub 2021/04/03. doi: 10.1073/pnas.2007194118. PubMed PMID: 33798093; PubMed Central PMCID: PMCPMC8000530.

76. Manieri E, Folgueira C, Rodriguez ME, Leiva-Vega L, Esteban-Lafuente L, Chen C, et al. JNK-mediated disruption of bile acid homeostasis promotes intrahepatic cholangiocarcinoma. Proc Natl Acad Sci U S A. 2020;117(28):16492-9. Epub 2020/07/01. doi: 10.1073/pnas.2002672117. PubMed PMID: 32601222; PubMed Central PMCID: PMCPMC7368313.

Supplemental Material Table of Contents

Supplemental Figure 1. Variation in Pkd2 mRNA levels is similar in Pkd2 mutant kidneys with or without Jnk.

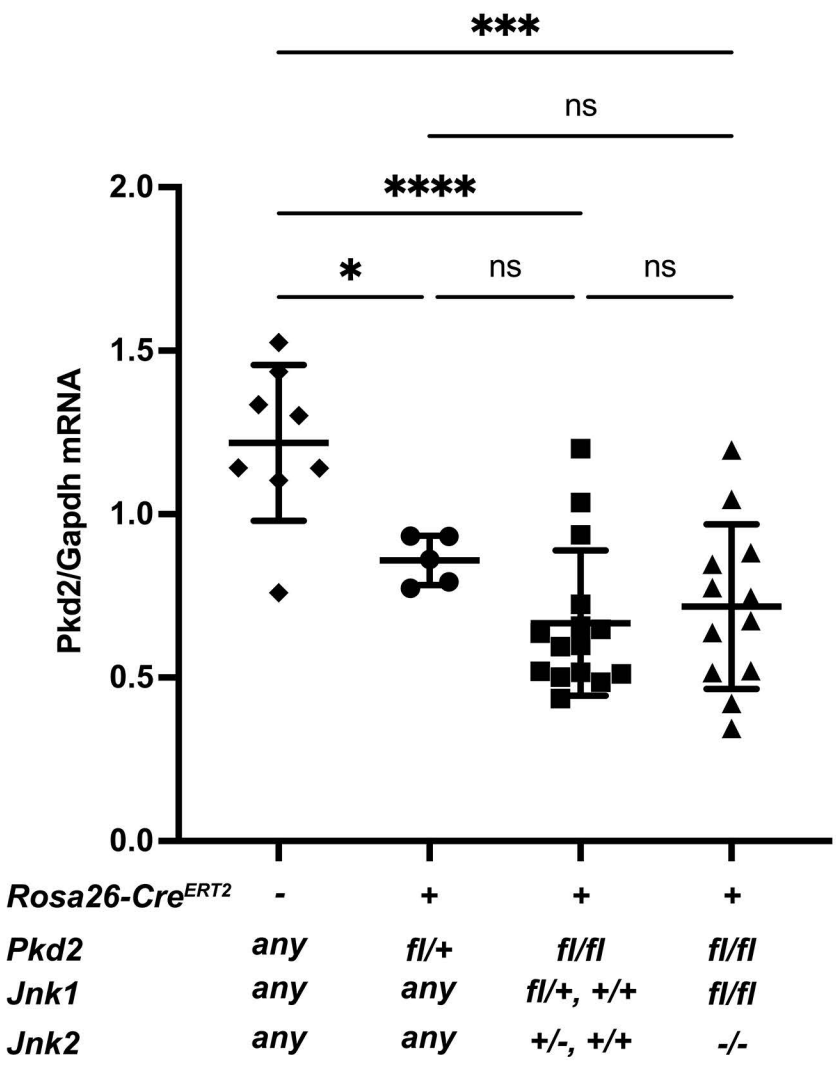

Supplemental Figure 1. Variation in *Pkd2* mRNA levels is similar in *Pkd2* mutants with or without Jnk.

(A) Total RNA was extracted from P21 kidneys. *Pkd2* mRNA levels were determined by RT-qPCR and normalized to *Gapdh*. All animals were treated with tamoxifen by maternal oral gavage on P2-4. The groups consist of Cre-negative animals (N = 8), *Pkd2* heterozygotes with any number of Jnk alleles (*Rosa26-Cre^{ERT2}; Pkd2$^{fl/+}$*) (N = 5)*, Pkd2* mutants with at least one wild type allele of *Jnk1* and *Jnk2* (*Rosa26-Cre^{ERT2}; Pkd2$^{fl/fl}$*) (N = 12), and *Pkd2* mutants with no functional *Jnk* alleles (*Rosa26-Cre^{ERT2}; Pkd2$^{fl/fl}$; Jnk1$^{fl/fl}$; Jnk2$^{null/null}$*) (N = 15). ****, P < 0.0001; ***, P < 0.001; *, <0.05; ns, not significant by one-way ANOVA followed by Tukey multiple comparison test with multiplicity-adjusted p-values. Error bars indicate SD.

Supplemental Figure 2. Loss of Ask1, Mlk2 or Mlk3 does not reduce kidney cysts in juvenile Pkd2 mutant mice.

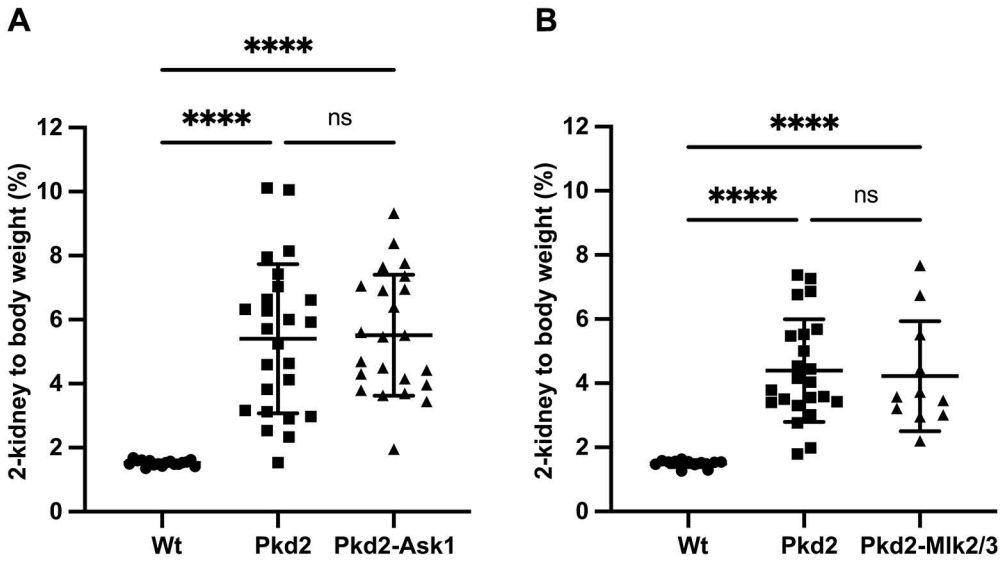

Supplemental Figure 2. Deletion of MAP3 Kinases *Ask1*, *Mlk2* and *Mlk3* is not sufficient to reduce kidney cysts in juvenile *Pkd2* mutant mice.

Mice with the following genotypes were treated with tamoxifen at P2-4 and collected at P21: Wt (*Rosa26-Cre^{ERT2}; Pkd2$^{fl/+}$*), Pkd2 (*Rosa26-Cre^{ERT2}; Pkd2$^{fl/fl}$*), Pkd2-Ask1 (*Rosa26-Cre^{ERT2}; Pkd2$^{fl/fl}$; Ask1$^{-/-}$*) and Pkd2-Mlk2/3 (*Rosa26-Cre^{ERT2}; Pkd2$^{fl/fl}$; Mlk2$^{-/-}$; Mlk3$^{-/-}$*).

(A) Cystic burden was quantified using the ratio of 2-kidney weight / body weight x 100%. N is 17 (Wt), 25 (Pkd2), 23 (Pkd2-Ask1). ****, P < 0.0001; ns, not significant by one-way ANOVA followed by Tukey multiple comparison test with multiplicity-adjusted p-values. Error bars indicate SD.

(B) Cystic burden was quantified using the ratio of 2-kidney weight / bodyweight x 100%. N is 12 (Wt), 23 (Pkd2), 11 (Pkd2-Mlk2/3). ****, P < 0.0001; ***, P < 0.001; ns, not significant by one-way ANOVA followed by Tukey multiple comparison test with multiplicity-adjusted p-values. Error bars indicate SD.

Supplemental Figure 3. Pkd2 loss induces phosphorylation of long and short Jnk isoforms.

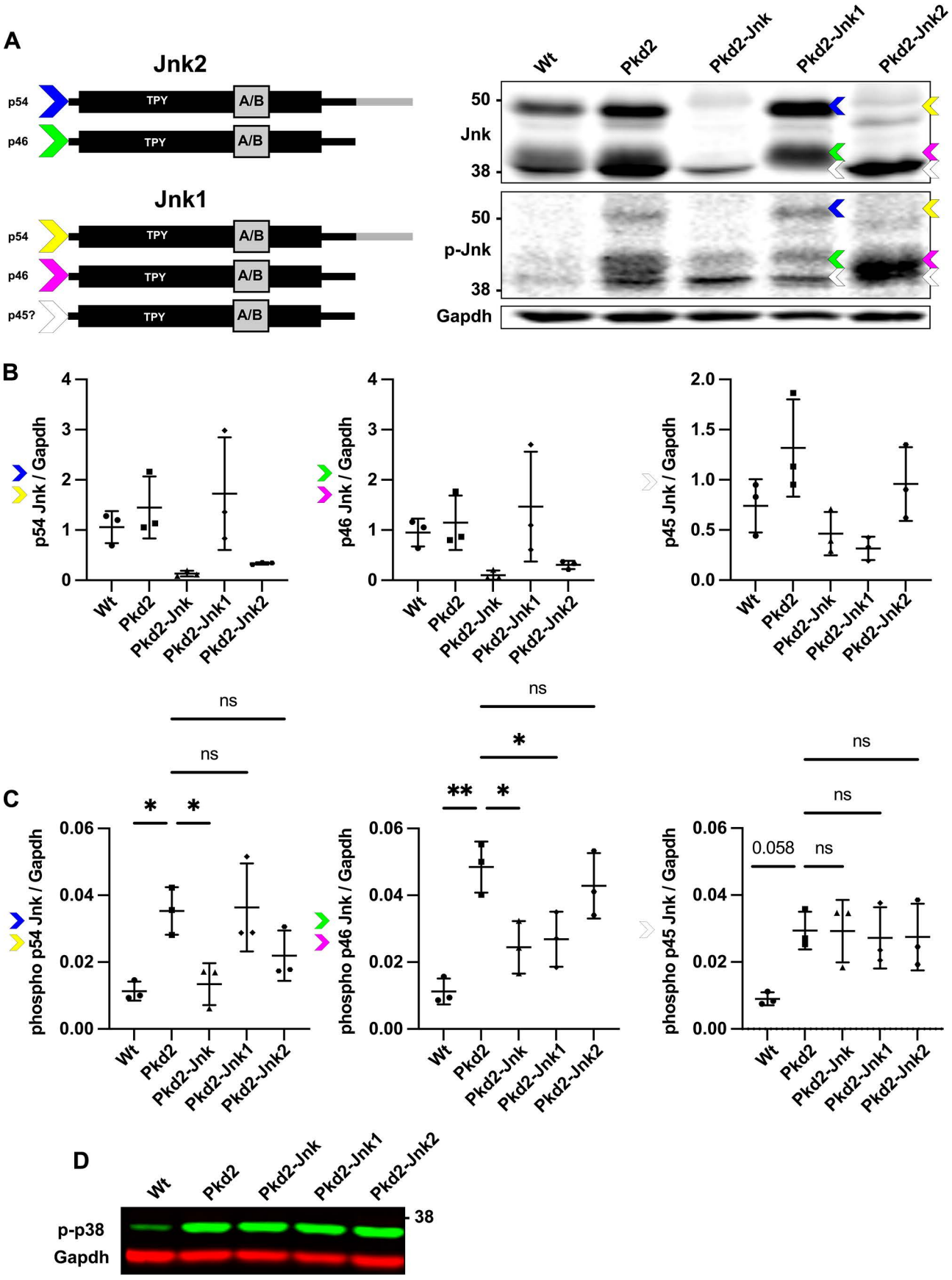

Supplemental Figure 3. *Pkd2* loss induces phosphorylation of long and short isoforms of *Jnk1* and *Jnk2*.

Mice described in Figure 2: Wt (*Rosa26-Cre^{ERT2}; Pkd2$^{fl/+}$*), Pkd2 (*Rosa26-Cre^{ERT2}; Pkd2$^{fl/fl}$; JNK1$^{+/+}$; Jnk2$^{+/+}$*), Pkd2-Jnk (*Rosa26-Cre^{ERT2}; Pkd2$^{fl/fl}$; Jnk1$^{fl/fl}$; Jnk2$^{null/null}$*)

Mice described in Figure 6: Pkd2-Jnk1 (*Rosa26-Cre^{ERT2}; Pkd2$^{fl/fl}$; Jnk1$^{null/null}$; Jnk2$^{+/+}$*); Pkd2-Jnk2 (*Rosa26-Cre^{ERT2}; Pkd2$^{fl/fl}$; JNK1$^{+/+}$; Jnk2$^{null/null}$*).

(A) Whole kidney protein lysates were immunoblotted for total Jnk, phospho T183/Y185 Jnk, and loading control Gapdh. The diagram (left) depicts the primary known isoforms of Jnk1 and Jnk2, as well as a putative isoform of Jnk1. Both Jnk1 and Jnk2 can be alternatively spliced to form four variants. Incorporation of the mutually exclusive exon pair 6a/6b in the kinase domain does not affect size of the protein, but alternative splicing at the C-terminus can produce either long (p54) or short (p46) forms that can be distinguished by immunoblot. Colored arrows indicate corresponding isoforms on the blot. These represent our predictions of which isoforms are present in each band. The white arrows correspond to a band of unknown identity (p45) which we quantified separately.

(B-C) Quantification of immunoblots described in (A). N is 3 animals per group. Due to low sample number, differences in total Jnk isoform levels did not reach statistical significance in most cases and are not displayed. For phosphorylated Jnk isoforms, we indicate the significance of each group compared to *Pkd2* mutants. Phospho-p45 nearly reached significance with p = 0.058. **, $P < 0.01$; *, $P < 0.05$; ns, not significant by one-way ANOVA followed by Tukey multiple comparison test with multiplicity-adjusted p-values. Error bars indicate SD.

(D) The kidney lysates described in (A) were immunoblotted for phospho T180/Y182 p38 and loading control Gapdh.

Supplemental Figure 4. Kidney cysts do not develop within 6 months of adult Pkd2 deletion.

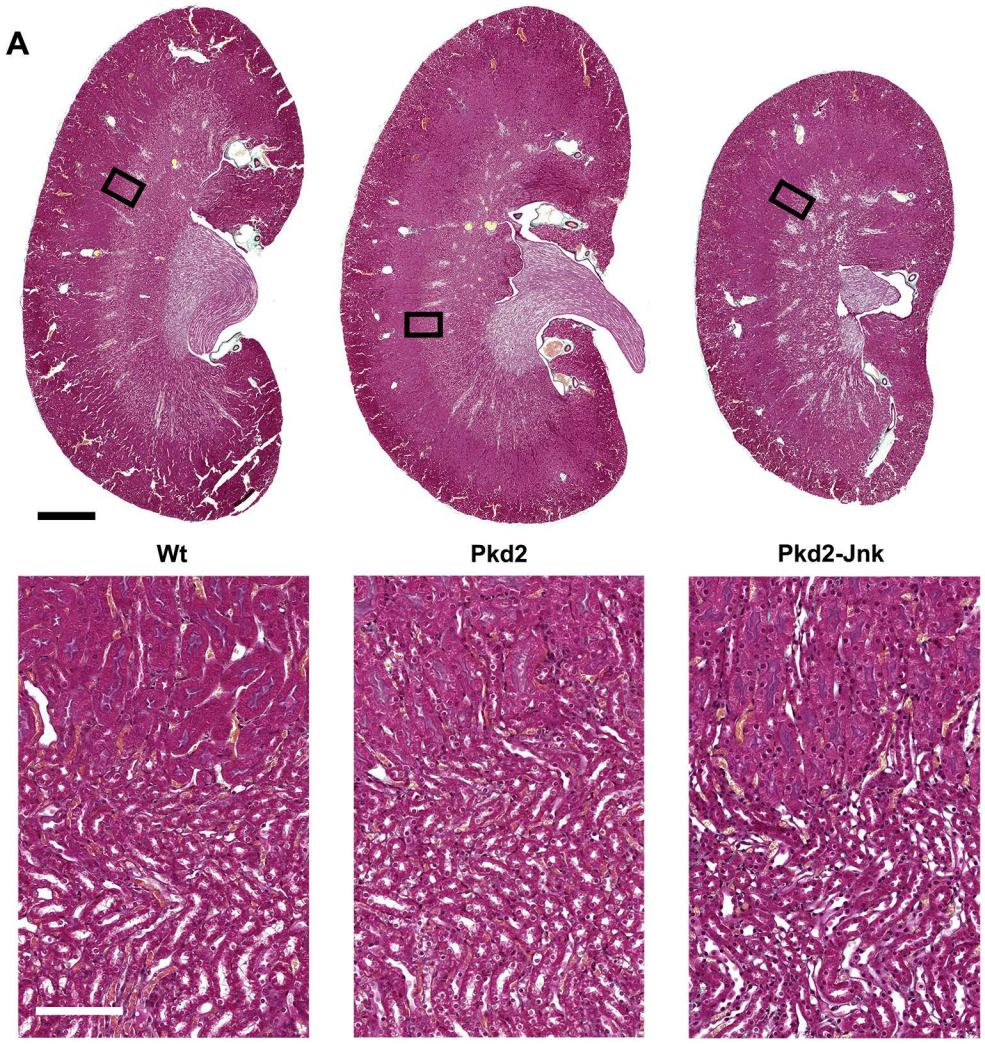

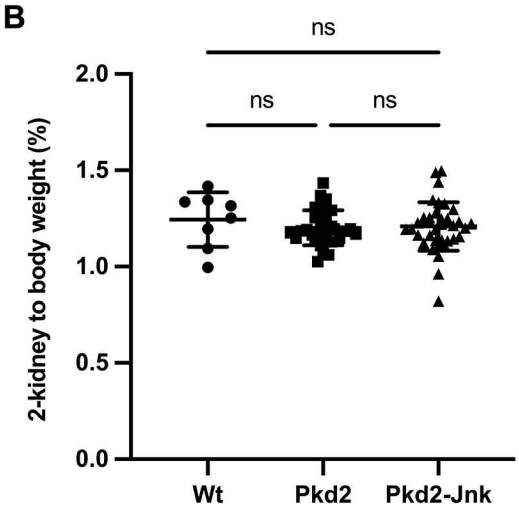

Supplemental Figure 4. Kidney cysts do not develop within 6 months of adult Pkd2 deletion.

Mice with the following genotypes were treated with tamoxifen at P21-23 and collected 24 weeks later: Wt (*Rosa26-Cre^{ERT2}; Pkd2$^{fl/+}$*), Pkd2 (*Rosa26-Cre^{ERT2}; Pkd2$^{fl/fl}$; Jnk1$^{+/+,\ fl/+}$; Jnk2$^{+/+,\ +/-}$*), Pkd2-Jnk (*Rosa26-Cre^{ERT2}; Pkd2$^{fl/fl}$; Jnk1$^{fl/fl}$; Jnk2$^{null/null}$*).

(A) Kidney sections were stained with one-step trichrome to mark collagen fibers pale green, cytoplasm red, and nuclei dark blue. Scale bar is 1000 microns for full size kidney scans, 100 microns for insets.

(B) Cystic burden in the kidney was quantified using the ratio of 2-kidney / body weight x 100%. N is 8 (Wt), 31 (Pkd2), 38 (Pkd2-Jnk). ns, not significant by one-way ANOVA followed by Tukey multiple comparison test with multiplicity-adjusted p-values. Error bars indicate SD.

Supplemental Figure 5. Sex does not influence severity of cystic phenotype in adult Pkd2 mutant mice.

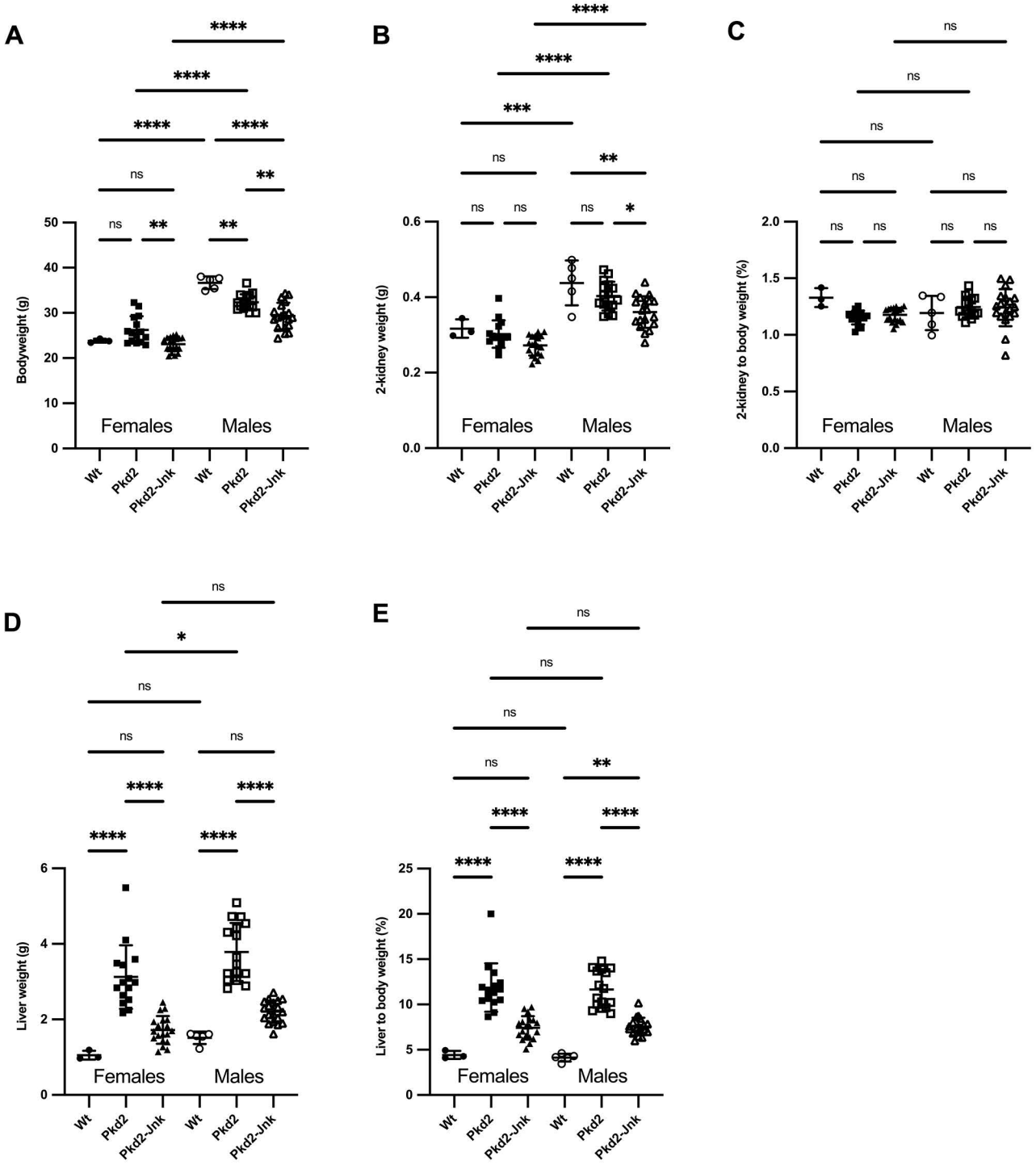

Supplemental Figure 5. Sex does not influence severity of cystic phenotype in adult *Pkd2* mutant mice.

Mice with the following genotypes were treated with tamoxifen at P21-23 and collected 24 weeks later: Wt (*Rosa26-Cre^{ERT2}; Pkd2$^{fl/+}$*), Pkd2 (*Rosa26-Cre^{ERT2}; Pkd2$^{fl/fl}$; Jnk1$^{+/+,\ fl/+}$; Jnk2$^{+/+,\ +/-}$*), Pkd2-Jnk (*Rosa26-Cre^{ERT2}; Pkd2$^{fl/fl}$; Jnk1$^{fl/fl}$; Jnk2$^{null/null}$*).

(A) Body weight of adult *Pkd2* mutant mice, segregated by sex. Females: N is 3 (Wt), 15 (Pkd2), 19 (PKD2-JNK). Males: N is 5 (Wt), 16 (Pkd2), 19 (Pkd2-Jnk). ****, P < 0.0001; **, P < 0.01; ns, not significant by one-way ANOVA followed by Tukey multiple comparison test with multiplicity-adjusted p-values. Error bars indicate SD.

(B-C) 2-kidney weight and 2-kidney to body weight (%) of adult *Pkd2* mutant mice, segregated by sex. Females: N is 3 (Wt), 15 (Pkd2), 19 (PKD2-JNK). Males: N is 5 (Wt), 16 (Pkd2), 19 (Pkd2-Jnk). ****, P < 0.0001; ***, P < 0.001; **, P < 0.01; *, P < 0.05; ns, not significant by one-way ANOVA followed by Tukey multiple comparison test with multiplicity-adjusted p-values. Error bars indicate SD.

(D-E) Liver weight and liver to body weight (%) of adult *Pkd2* mutant mice, segregated by sex. Females: Females: N is 3 (Wt), 15 (Pkd2), 19 (PKD2-JNK). Males: N is 5 (Wt), 16 (Pkd2), 19 (Pkd2-Jnk). ****, P < 0.0001; **, P < 0.01; ns, not significant by one-way ANOVA followed by Tukey multiple comparison test with multiplicity-adjusted p-values. Error bars indicate SD.